UNIVERSITY OF ARKANSAS

Graduate Institute of Technology

CONTRIBUTIONS OF SYSTEM PARAMETERS IN THE DOPPLER METHOD OF FLUID VELOCITY DETERMINATION

CONTRIBUTIONS OF SYSTEM PARAMETERS IN THE DOPPLER METHOD OF FLUID VELOCITY DETERMINATION

CONTRIBUTIONS OF SYSTEM PARAMETERS IN THE DOPPLER METHOD OF FLUID VELOCITY DETERMINATION

A dissertation submitted in partial fulfillment
of the requirements for the degree of
Doctor of Philosophy

By

ROBERT LEVI BOND, B.S., M.S.
State College of Arkansas, 1961
University of Arkansas, 1964

1968
The University of Arkansas

This dissertation is
approved for recommendation
to the Graduate Council

Major Professor:

Dissertation Committee:

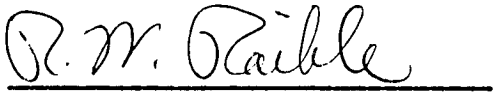

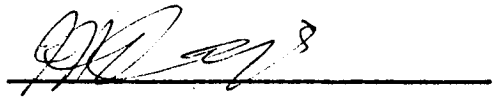

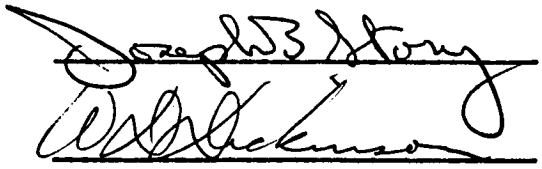

ACKNOWLEDGMENTS

I would like to express my appreciation to Dr. M. K. Testerman for his faithful pursuit of all legitimate methods to assure that I could complete the degree associated with this dissertation. He acted well beyond his responsibilities as Major Professor, not only in pre-empting two consecutive holiday weekends to work on the rough draft of this dissertation but also in giving moral support and suggestions.

I would also like to thank Dr. Joseph B. Story who as research director gave a great deal of his time and effort to supervising the research and to working out the initial problems in the rough draft of this dissertation. In addition, I sincerely thank Mr. Raymond W. Raible, Dr. T. A. Raju, and Mr. Dewoody Dickinson for waiving the normal time limits allowed for reading the dissertation and for taking time from their busy schedules to appear on my oral committee.

I thank Mrs. Rita Roller who for the second time has used her unique abilities to prepare the final draft of a thesis before the onrushing deadline. I also thank my mother and sister who have made great sacrifices to enable me to be in the position to write this at all. I thank Mr. David Wankum for his contributions to this research effort.

This work was partially supported by Research Grant NGR-04-001-015 from the National Aeronautics and Space Administration.

TABLE OF CONTENTS

LIST OF TABLES

TABLE

LIST OF FIGURES

FIGURE

CONTRIBUTIONS OF SYSTEM PARAMETERS IN THE DOPPLER METHOD OF FLUID VELOCITY DETERMINATION

I. INTRODUCTION AND BACKGROUND

A hydrodynamic problem has arisen in the use of high-thrust rocket engines with multiple nozzles. The flow pattern is such that the hot exhaust gases are circulated against the base of the rocket. The heating of the rocket base must be considered if a satisfactory heat balance is to be maintained. It is desirable to know the detailed flow configuration about the base of the rocket.

The determination of fluid flow patterns in the past has been limited in accuracy by the disturbances caused by the measuring probes themselves or by incomplete data in the case of optical methods. Mechanical devices are limited in frequency response. Hot wire or hot film anemometers have been used extensively in the past but the thermal time constants of these devices limit the frequency response to 200 kHz at best for a 3 db drop in signal level. In addition, the probes are mechanically fragile, particularly those for high frequencies, and cannot be easily applied to the determination of contaminated flow or to very-high velocity flow.

The hot wire anemometer can be used in pure air up to velocities of 200 m/sec without mechanical failure. In contaminated flow a coating rapidly develops which causes erroneous readings. In abrasive flow the thin film or wire rapidly erodes,

producing reading errors and eventual failure of the probe. The hot film anemometer can be used in air at velocities (at atmospheric pressure) slightly above 500 m/sec and in some liquids up to 7 m/sec. The maximum temperature at which these probes can operate is approximately 150°C. The sizes of these probes are considerably larger than the diffraction limited focus of a laser beam since the minimum length is usually between 0.5 and 1.0 mm.

The Pitot tube is limited in the determination of high-speed fluid flow since its time constant is long because of the inertia of the fluid in the readout device. It is larger than the anemometers (∿3mm diameter), it tends to perturb the fluid flow to a greater extent, and it is prone to errors introduced through contamination and cannot be used when solids exist in the fluid flow.

Optical systems (schlieren, interferometry, shadowgraph) used in the study of fluid dynamics are usually limited practically to laboratory situations in which their environment is closely controlled. Although these measurement techniques do not perturb the flowing system, it is extremely difficult to get quantitative information concerning the particular dynamics of a flowing system, especially for a high frequency turbulent medium. An additional problem with measurements on hot flowing systems, such as those around rocket bases and jets, is the high background optical noise generated by the gases themselves.

All of the above techniques for the study of fluid dynamics suffer from the inability to measure localized flow. That is, all of the systems are flow integrators because of their large sampling volumes.

When the relative merits and disadvantages of the above techniques for fluid flow determination are considered, the conclusion is that a specialized optical system is preferable since photons will not perturb the flow and a beam of light can be focused to an extremely small spot giving a small sampling volume. This suggests using the shifted optical Doppler signal scattered from the spot focused in the flowing system. However, until recently no technique existed for detecting this shifted signal. The spectrographs used in astronomical Doppler measurements lacked several decades having sufficient resolution. The heterodyne techniques used in microwave frequency radars could not be used because of the incoherence of optical sources as well as their lack of intensity when made sufficiently monochromatic.

The advent of the continuous wave laser provided both a suitably coherent, monochromatic, and intense source as well as a detector. This combination permits evaluation of flow patterns with minimal interaction between the photon primary transducer and the flowing system.

The coherence and monochromaticity of the laser beam probe permit mixing of the Doppler frequency-shifted radiation scattered from a dynamic fluid system with a known optical frequency (local

oscillator) to obtain a sufficiently low beat frequency that can be detected with optoelectronic devices.

This phenomenon is completely analogous to frequency mixing at radio-frequencies and is therefore called optical heterodyning. This modulated optical wave is transformed into an electrical signal by a high-sensitivity square law detector according to

$$i = \alpha_o + \alpha_1 E^2 \qquad (1)$$

where i is the current generated in the photodetector, E is the amplitude of the optical signal, and α_o and α_1 are the first two constants in the Fourier expansion. Higher terms are insignificant. The output of the nonlinear optical detector may be represented on the intensity versus frequency scale of a spectrum analyzer as a signal with a probability distribution function which should be a measure of the velocity fluctuation distribution in a given scattering volume. Of course, in practice more advanced readout techniques would be necessary for turbulent flow.

The correlation between this probability distribution function and the velocity of a flowing fluid has been established through the Doppler equation for one-dimensional laminar flow (6). In this work it was found that particle velocities could be measured by focusing a laser within a gas stream containing suspended particles. The light scattered from this focal region at a particular angle to the incident beam was recombined with a portion of the incident beam to produce the heterodyne signal. The interpretation of the heterodyne signal was contingent upon the viscous nature of the flow. In this simple case the flow was

assumed to be along a single axis and the velocity vector $\vec{v}$ reduced to a simple scaler, speed v_n, along a known axis. Since the velocity at any fixed point in the flowing system was time invariant as to direction, a single measurement of speed completely analyzed the flow pattern at the fixed point. The distribution function as seen by a spectrum analyzer would be caused in part by the distribution of velocities in the finite sampling volume. A goal of this dissertation was to determine which system parameters contributed to the readout and specifically what caused the spread in the distribution function. This goal would be particularly important in the projected use of the device for measuring velocity vectors in three-dimensional turbulent flow.

In particular the causes of frequency and intensity fluctuations in the distribution function; the size, size distribution, density of distribution of the scattering centers; the size and effect of the scattering volume; and certain interactions were investigated. Scattering centers had to be produced that fulfilled theoretically and empirically determined criteria. They were chosen carefully to prevent severe nonlinear interactions which would invalidate the acquired data: particles that were too heavy or large would not follow the flow pattern, particles that had large size distributions (polydisperse) would have a velocity distribution of their own, particles that absorbed highly would be poor scatterers, and particles that were too small would have low scattering

efficiencies. In order to meet these criteria the properties of the particles had to be known and these characteristics had to be reproducible.

The determination of the effect and size of the scattering area and later of the scattering volume had to be made. The size of this scattering center (in the broad sense) had to be optimized in relation to the other parameters of the system and with respect to the degree of turbulence. The center could be so small that the only data taken would be noise representing microscopic fluctuations. Conversely, if the center were too large, the data would be integrated over a given area and would not give the true value of localized turbulence.

The one-dimensional scattered radiation was studied relative to data reduction, interpretation and sampling techniques. The readout of the data was also studied. The degree of contribution of the experimental setup itself to the data was ascertained. Undesirable effects could then be eliminated, minimized, or corrected for in the readout of the data. The desirable effects could be amplified, and the entire system optimized. The study was limited to simulated flowing systems and flowing liquids. A more detailed discussion of the approach to the problem as well as the results are presented in the following dissertation. The chief contributions of this study are related to the symmetrical heterodyne arrangement, to the understanding gained of the parameters, and to the optimization of the heterodyne technique for velocity measurement.

II. LITERATURE SURVEY

The optical heterodyne technique of velocity measurement was developed by Yea and Cummins (17) to study a wide range of flow rates in flowing liquid systems. The technique was subsequently applied to flowing gas systems by Foreman, et al. (6). The latter researchers have published widely concerning the basic operation of the "laser velocimeter", as the instrument is called by them. However, there has been little effort made to understand the coordination between the physical characteristics of the instrument and the resultant readout. Furthermore, the system has not been optimized for the type of studies for which it was originally designed. For example, all previous researchers have used forward scattered light which leads to a geometrically difficult configuration in relation to the studies of the total rocket exhaust problem. In addition for studies of three-dimensional flow several velocimeters would be necessary for complete analyses. According to van de Hulst (15), the use of the backscattered radiation would have a disadvantage as related to the intensity of the received radiation. However, the nominal ten-to-one front-to-back ratio of the scattered radiation does not place unrealizable constraints on the receiving system.

Several authors (12, 13, 8) have given theoretical and experimental treatments of the characteristics of coherent radiation backscattered from optically inhomogenous secondary radiators — both static and dynamic. As will be seen later, the

particulate composition of the secondary radiators can be limited to the Mie scattering region (i.e. particles with diameters between 0.1μ and 100μ. The Mie theory of spherical particles (11) coupled with that developed by other researchers leads to a concept of large backscattered lobes of radiation modulated by smaller lobes caused by the coherence of the incident radiation. The result is a speckle pattern which has an intensity gradient dependent upon the location of a given sampling area in relation to the Mie scattering lobes.

Recently Goldstein and Kreid (7) used the Doppler flowmeter to study the development of laminar flow in a square duct. They used forward scattered radiation in an unusual experimental arrangement in which two beams were brought together at a single focal point.

III. THEORY

A. Study of Scattering Centers

In using the scattering from a flowing system, the magnitude of the scattered radiation is extremely important. The scattering can occur at density gradients in the flowing fluid, from molecules and/or atoms of the flowing fluid itself, or the scattering may occur from natural or artifically introduced impurities in the flowing stream. Some properties of scattering will be considered before concluding which scattering medium would be most suitable for this study. The selection of a suitable scattering medium is of primary importance in the development of sufficiently intense scattering and of the desired angular distribution of this scattered radiation. Polarization effects must also be included in this search for appropriate scatterers.

Scattering is usually classified into two main divisions — dependent and independent. Independent scattering occurs when the scattering of a given particle is not coupled to the scattering of any neighboring particles. This criterion is determined solely by particle separation and is met when the separation is about three times the particle radius (15).

Additionally, scattering may be classified as to the relationship between the frequency of incident and scattered radiation. In some cases (Raman scattering for example) there are actual quantum transitions in which there is a loss or gain in the frequency of the scattered photon. This quantum effect must not be confused with the Doppler frequency shift in which energy is

conserved without absorption or emission of additional quanta. This study was limited to radiation that is not fundamentally shifted upon scattering.

Scattering may also be classified according to the sizes of the particles from which the scattering occurs. In these types of scattering the frequency is not changed. There are three basic photon-matter interactions that in a broad sense may be classified under scattering:

1. Reflection $\lambda << d$
2. Rayleigh or Thompson Scattering $\lambda >> d$
3. Mie Scattering $\lambda \approx d$,

where λ is the wavelength of the incident radiation in the suspending medium and d is the diameter of the scattering particles.

1. Reflection. In pure reflection the mechanical inhomogeneities are large enough that there are broad areas that appear optically flat to the incident radiation, wherein the phases of scattered light from adjacent particles will agree. The secondary waves from the atoms in the surface will cooperate to produce a reflected wave front traveling at an angle equal to the angle of incidence. Since the wavelets are additive, the scattered (reflected) wave approaches the intensity of the incident ray. Losses are primarily caused by conversion of some of the electromagnetic vibration energy into heat (absorption) rather than re-radiating it as visible light. For monochromatic light it is relatively simple to construct surfaces that have a visible wave radiation) extinction

coefficient that consists of less than 0.1 percent absorption. Therefore, this system is highly efficient. The mathematical description of such a system is simple:

$$\phi = \phi' \tag{2}$$

where ϕ is the angle the incident radiation makes with the normal to the scattering particle and ϕ' is the angle the scattered radiation makes with the normal. It will be noted that the scattered radiation from a perfect reflector (i.e. $d = \infty$) forms a beam that is the same diameter as the incident beam except for minimal diffraction effects caused by the laser exit aperture. That is, the scattering cross section for a beam of cross sectional area of 1.0 cm^2 approaches 1.0 cm^2.

As d becomes of the order of magnitude of the beam diameter, the scattering is no longer ideal reflection and there is a three-dimensional intensity distribution about the angle ϕ'. This radiation packet, called a lobe, becomes important in other types of scattering.

Because of the high scattering efficiency and simple theory associated with pure reflection, it would be highly desirable to utilize it in this study. However, there are two major factors which prevent its use. Since the result of the studies will ultimately be applied to turbulent systems, the particles must have spherical symmetry to present the same scattering profile to the incident beam at all times since the particle orientations are time variant in turbulent flow. However, with this shape the

particle must have a large cross section to meet the criterion of flatness discussed above and as a result will have a large mass. This large mass would preclude the particle following the fluid flow accurately. If the particle were 1.0 mm in diameter, it would follow the law of reflection to an extent, but even if it were a water droplet with its low density, it could not follow the fluid motion into the turbulent region of flow. Highly reflective dielectrics or metals would indeed have prohibitive particle masses, the latter not following the highest viscous flow but falling to the bottom of the flow channel. That is, with the best pure reflectors nothing more than integration of the turbulent flow into a generalized velocity vector along the net mass-flow direction could be expected. Therefore, it is evident that reflection cannot be used.

2. Rayleigh or Thompson Scattering. Thompson scattering occurs as a result of interaction of electromagnetic radiation with free electrons. The scattering cross section is of the order of 10^{-26} cm^2 as given by

$$\frac{I}{I_o} \approx \frac{8\pi r^2}{3}. \qquad (3)$$

Here r is the radius of scattering particles, I is the intensity of the scattered radiation and I_o is the intensity of the incident radiation. Thompson scattering depends upon the available free electrons which in turn depend upon the degree of ionization of the atoms and molecules in the fluid. It must be noted that this makes the degree of scattering temperature sensitive because of the relationship between numbers of ions produced and the temperature

of the Maxwellian gas. Therefore, because of the small scattering cross section for electrons and the statistical variations in their number, the theoretically simple Thompson scattering cannot be used.

Scattering from randomly distributed molecules and atoms has an intensity factor that is at least three orders of magnitude below that for Thompson scattering. This phenomenon, called Rayleigh scattering, can be described simply in mathematical terms. The intensity relationship is given by:

$$I/I_o = kV^2\lambda^{-4} \tag{4}$$

where V = volume of a scattering particle

λ = wavelength of the incident radiation

k = proportionality constant

I/I_o = the scattering cross section for random scatterers.

For random scatterers the total scattered intensity in any direction is determined by summing the <u>intensities</u> of all scattered waves. For ordered scatterers the <u>amplitudes</u> are additive. The value as a function of observation angle, θ, is

$$I(\theta) \propto \tfrac{1}{2}(1 + \cos^2\theta) \tag{5}$$

which is symmetrical about $\theta = \pi/2$.

The scattering cross section at any observation angle becomes

$$\frac{I(\theta)}{I_o} = NV_n \left(\frac{2\pi n_o}{\lambda}\right)^4 \frac{\alpha^4}{x^2} \frac{1}{2} (1 + \cos^2\theta) \tag{6}$$

where $\frac{I(\theta)}{I_o}$ = scattering cross section for a given observation angle, θ

N = number of scatterers per unit volume

V_n = total scattering volume

n_o = refractive index of medium

λ = vacuum wavelength of incident radiation

α = polarizability tensor

x = distance from scattering center to optical receiver

For anisotropic scatterers this equation is complicated by the necessity for taking the mean of the three principal values of the polarizability tensor as well as by a polynomial ratio containing a depolarization coefficient.

In random scatterers the total scattered intensity is directly proportional to the number of scatterers since the resultant amplitude is proportional to the square root of the number of scatterers. In randomly distributed particles smaller than λ the amplitude is directly proportional to the number of scatterers (proportional to mass) and therefore the intensity is proportional to the square of the number of scatterers. for independent scatterers.

The total light power scattered through 4π steradians from unit volume and unit incident intensity across a sphere of radius r is called the scattering coefficient, τ

$$\tau = \frac{4\pi}{3}\left(\frac{2\pi}{\lambda'}\right)^4 N\alpha^2. \qquad (7)$$

The relation of intensity to observation angle is simple and is symmetrical about a plane through the scatterer and perpendicular to the incident radiation. The degree of polarization can be stated in simple terms as:

$$P(\theta) = \frac{\sin^2\theta}{1 + \cos^2\theta} \qquad (8)$$

where P (θ) = degree of polarization (varying from a maximum of unity at $\theta = 90^{\circ}$ to a minimum of zero at $\theta = 0^{\circ}$) and where θ = angle of observation. The desirability of using this type of scattering from a theoretical standpoint is negated, however, by the extremely small scattering cross section of approximately 10^{-29} cm^2.

Scattering in the case of spontaneous fluctuations of density in a homogeneous medium also comes under the Rayleigh scattering theory and therefore suffers from the same lack of intensity.

In general, the above scattering theories hold only for particles whose diameters are considerably less than the wavelength of the incident radiation. Of course, it would be desirable to use the particles (atoms, molecules, electrons or density fluctuations) of the flowing medium since they would of necessity follow the eddies of turbulent flow as well as less time variant laminar flows.

It would also be possible to utilize higher power lasers to get higher intensity scattered radiation. However, there are several disadvantages to taking this approach. First, most lasers of high intensity operate in the pulsed mode, making it impossible to have a continuous signal readout. In addition, when the radiation is focused to produce a small sampling volume, several disruptive effects occur. If the power density coupled with the electrical field strength is sufficiently high (as it almost always will be) the flowing gases will be multiply ionized with a great deal of force, causing a severe loss of optical coherence and a disruption of the turbulence pattern. Even with rather low power

pulses there is a significant thermal effect between the particles of the fluid and the incident photons. Also, there can be a significant photon pressure at high intensities of radiation. In other words, with the use of high power lasers the pertubation caused by the non-linear photon-matter interactions could be more disruptive to flow patterns than standard mechanical probes. It will be shown later that these effects are negligible for a 50 mW cw laser.

Low power, continuous CO_2 lasers could also be used since their output could be made low enough to minimize most non-linear photon-matter interactions. However, the increase in scattered intensity would be negated by the low quantum efficiencies of photo-detectors at the CO_2 line of 10.6 microns. Thermopiles which are normally used in this spectral region would not have sufficient frequency response to be used.

There are also considerable safety hazards associated with the use of either high power pulsed lasers or the continuous CO_2 laser. The latter poses a particular safety problem because of its invisible output.

3. Mie Scattering. A segment of the particle size region ($0.1\ \mu < d < 100\mu$)(i.e. $d \approx \lambda$) between Rayleigh scattering theory and pure reflection cannot be treated by either of these simple theories. The theory in this region is extremely complex and has been given in detail only for perfectly spherical particles (11).

Mie treated scattering from spherical particles as an electromagnetic wave boundary-value problem. The scattered wave amplitudes are determined as infinite series of Bessel functions of the radius multiplied by spherical harmonics in the observation angle. The scattering depends upon the ratio of the refractive index of the sphere to that of the medium in which the sphere is suspended $m = n_1/n_o$; upon the size of the sphere (radius = r); upon the wavelength of light in the medium ($\lambda' = \lambda/n_o$); and upon a coefficient $y = 2\pi r/\lambda'$. As $\frac{n_1}{n_o} \cdot \frac{2\pi r}{\lambda'}$ approaches zero (i.e. $r \to 0$ as in Rayleigh scattering) all the terms of the series except the first vanishes, giving the classical Rayleigh equation for re-radiation from the induced electric-dipole moment in the scatterer.

As a second approximation to scattering, the induced electric-quadrupole and magnetic moments are included. This approximation is good to a value of $r \simeq \lambda/6$ and $m \simeq 1.33$ (H_2O droplets in air). The degree of polarization with angle becomes a two-component series expansion even for this simple approximation.

As the particle size increases, the scattering intensity also increases, but the mathematical complexity also increases as more terms in the Bessel series become necessary to describe the scattered radiation.

In the region of the second approximation the scattering becomes asymmetric with the forward scattering lobe more intense than the back scattered lobe. In addition, the light is depolarized to an extent at $\theta = \pi/2$ for both isotropic and anisotropic scatterers.

The scattering coefficient is given by

$$\tau = N \pi r^2 f(y) \tag{9}$$

where $y = 2\pi r/\lambda'$ as given before. The function $f(y)$ is extremely complex but has the following limiting values

$y << 1$	$f(y)$ related to y^4 and λ^{-4}	
$y \approx 1$	$f(y)$ related to y^2 and λ^{-2}	
$y >> 1$	approaches value of 2.	(10)

For $y << 1$, the function $f(y)$ is simply Rayleigh's 4-power law. As the particles become large (Mie scattering) the scattering is independent of wavelength in the limit.

Mie theory also holds for electrically conducting particles if the complex refractive index of the conducting particle is used. Metals scatter more in the back direction than in the forward direction. Also, the value of the complex index (both coefficients) of refraction decreases with increasing wavelength such that scattering is more efficient toward the ultraviolet end of the optical spectrum.

In the Rayleigh scattering region the scattering is spherical and of small intensity. When the size of the particle becomes sufficiently large that the phase differences between light scattered by its various parts becomes significant, the amplitudes are no longer purely additive. This phase difference is maximum for back scattered light and extinction occurs at $r = \lambda/4$ and $\Theta = \pi$. That is, as the particle size increases, the forward scattering increases as r^2, while the backscattering decreases

to zero at $r = \lambda/4$. As r becomes still larger, extinction occurs at $\pi/2<\theta<\pi$ and the lobe along $\theta = \pi$ becomes more intense. At larger values of r the intensity of the backward lobe reaches a maximum (at about $2\pi r/\lambda = 2.4$) and eventually moves over to $\pi/2<\theta<\pi$ ($2\pi r/\lambda > 3.0$).

As the particle size is increased, the total scattered intensity increases dramatically (about 10,000 as $2\pi r/\lambda$ changes from 0.5 to 6.0 for example). Also, the number of lobes increases from one at $2\pi r/\lambda = 0.5$ to several dozen as $2\pi r/\lambda$ approaches 10. Obviously the number and position of these lobes depend on the ratio r/λ.

If these large particles are randomly distributed, the intensities add directly, if the criteria for independent scattering holds. The scattering intensity is greater than 10^{17} times that for Rayleigh scattering. Mie scattering depends upon the nature of the particles, their size and distribution. In general, if the particles are sufficiently larger than the wavelength of the incident radiation, the scattering is independent of wavelength. Mie scattering theory is complicated because it is a combination of diffraction theory and diffuse reflection theory (2). An additional intensity factor is gained in the larger particle scattering region where $f(y) \to 2$, since the scattering cross section is equal to twice the geometrical cross section. Half this amount corresponds to scattering through large angles and the other half corresponds to scattering through extremely small angles (4).

Mie scattering amplitude depends upon the electrical conducting properties, the observation angle, and the intensity of incident

radiation in addition to the factors discussed above. From insulating particles the scattered radiation is polarized elliptically and the major $\vec{E}$ vector of the ellipse is rotated oppositely on either side of the incident beam. The value of the polarization is independent of the mode of polarization of the incident beam for small angles.

Mie scattering from homogeneous, transparent, isotropic spherical particles is now discussed with particular regard to the scattered intensity as a function of the angle between the plane of polarization of the incident beam and the plane defined by the incident and scattered ray directions (called α here), and to the degree and plane of polarization of the scattered light (5).

(1) The plane of polarization of the light scattered from spherical, homogeneous, optically inactive particles of arbitrary size (such as water droplets) will be the same as if a portion of the incident beam had simply been reflected by an ideal mirror placed at the particle position. Thus, in heterodyne experiments the polarization of the referenced beam and of the scattered beam will always be the same at the photomultiplier as long as the scattering particles have the properties listed above.

(2) The intensity of scattered light will generally depend upon the angle between the plane of polarization of the incident beam and the plane defined by the incident and scattered ray directions.

A general exception to the second rule occurs if the index of refraction of the particle is sufficiently large. In this case

the scattered intensity is isotropic about the incident ray direction.

Approximate exceptions also occur for particular particle sizes, which depend upon the index of refraction of the substance and the wavelength of the irradiating light. For example, water droplets of 0.2μ radius will scatter 6328 Å light isotropically about the incident beam direction. Polystyrene spheres of 0.25μ radius will behave similarly.

A special case is that of backscattering. Since the angle θ between the incident and scattered rays is 180° for backscattering, the scattered intensity cannot be a function of α. This is a perfectly general statement, and is also true of course for forward scattering ($\theta = 0^{\circ}$).

Mie scattering is practically independent of the wavelength of the incident radiation, especially in the larger particle sizes. For metallic particles the scattered radiation is dependent on the mode of polarization of the incident radiation. If the incident radiation is linearly polarized the polarization of the scattered radiation is conserved.

Therefore, Mie scattering (or more accurately, modifications of Mie scattering) is a rather undesirable but necessary compromise for the present study. Any deviation of the particles from a spherical configuration or any distribution in particle sizes complicates Mie theory to the extent that it is useless. The difficulty of theoretically analyzing this type of scattering

suggested that a direct experimental attack was desirable. In fact most of the studies of scattering from particles of Mie dimensions have resulted in tedious tabulation of the intensity and polarization functions in relation to the particle diameter-wavelength ratio, angle of observation and other pertinent parameters.

B. Miscellaneous Effects. There are several phenomena that occur when photons come in contact with material particles. The effects of these phenomena in relation to these studies are now considered.

1. Power Density. The power concentration of a 50 mW laser beam focused to its diffraction limit is given by

$$S = \frac{AP}{\lambda^2 f^2} = \frac{(0.1257\ cm^2)(50\ mW)}{(0.6328 \times 10^{-4} cm)^2\ (40\ cm^2)} \qquad (11)$$

$$\approx 90\ W/cm^2$$

where A = area of transmitting antenna (laser beam diameter)

P = transmitted power (output of laser)

λ = vacuum wavelength of transmitted radiation

f = focal length of focusing lens

S = power density at focal point.

This was experimentally shown to be sufficient power to melt low-melting polymers.

2. Radiation Pressure. If a particle having a radius of 5_μ, for example, undergoes collision with a beam of power density 90 W/cm^2, the force exerted on the particle is 3×10^{-19} newtons. The equivalent acceleration of this particle is 5×10^{-4} mm/sec^2 which is insignificant as compared to the values under consideration.

3. Field Strength. The field strength existing at the focal point is given by

$$F = (120\pi\ S)^{\frac{1}{2}}$$
$$= (120\ \pi .\ 90\ W/cm^2)^{\frac{1}{2}}$$
$$= 184\ V/cm. \qquad (12)$$

This magnitude of field strnegth is not sufficient to disrupt the normal linear optical processes occurring at the focal point, since the binding strength in the material is of the order of 10^8 V/cm (2).

4. Doppler Energy Equivalence. The Doppler signal is seen as a frequency shift. At a given angle of observation this corresponds to a well defined energy increment

$$E = hf_1 - hf_2 = hf_D \qquad (13)$$

where E = energy equivalent

h = Planck's constant

f_D = Doppler frequency shift.

At a Doppler frequency of 10 MHz the equivalent observed energy shift is

$$E = (6.6 \times 10^{-27}\ erg\ sec)\ (10 \times 10^6\ Hz)$$
$$= 66 \times 10^{-21}\ ergs$$

which is in the range of translational energies, and is therefore insignificant.

IV. EQUIPMENT

A. Introduction. Equipment which was used throughout the experimental studies will be described below. Equipment that was used only on specific studies will be described under those studies. Several instruments of a given kind were used interchangeably depending upon which factor was being stressed. Therefore, they will all be described.

1. Radiation Source. The light sources used in this study were helium-neon lasers operating continuously in the TEM_{oo} mode with plane-polarized output and emitting a single wavelength of 6328 Å. During the study four different lasers were used with specifications given in Table 1. Of course, the power output of the lasers varied with time because of the inherently short lifetime of the plasma tubes. The power was measured with a Spectra-Physics Model 401B power meter.

2. Spectrum Analysers. The majority of data was readout on spectrum analyzers. A Singer Model SPA-3/25a spectrum analyzer was usually used, but two other instruments were used in certain frequency ranges. These were Tektronix 1L10 and 1L20 spectrum analyzers. The salient characteristics of the three spectrum analyzers which were used are shown in Table 2. The above values are inter-related and therefore the value of one depends upon the setting of others. These values were measured at half peak height. Generally the value is increased by 2.0 at 5 percent of total peak height. The Singer spectrum analyzer has an input impedance

of 72 ohms; the two Tektronix instruments have an input impedance of 50 ohms.

The sweep rate is a major problem with the Tektronix spectrum analyzers used in Tektronix 585 oscilloscopes. At low sweep rates the resolution is maintained, but phosphorescence of the CRT screen is too short to study the display well; at higher sweep rates where the CRT display is acceptable, the resolution and, therefore, peak amplitude deteriorate.

3. Photodetectors. The optically mixed beams were heterodyned on the photocathode of a photomultiplier. Three different multipliers were used at various times during the studies. Table 3 lists the pertinent information for these photomultipliers. The data were taken at approximately 25°C.

A 50 ohm load resistor is used to increase frequency response and to match the input impedances of the spectrum analyzers and the amplifier.

The high voltage (Model 405B manufactured by John Fluke, Inc.) D.C. power supply for the photomultiplier is highly regulated (0.001 percent), has high thermal stability (20 ppm/°C), and has good long-term drift characteristics (± 0.005 percent/hour, ± 0.03 percent/day). The voltage divider consists of zener diodes bypassed by low values of capacitance to permit stable operation at both high and low frequencies. The zener diode divider permits a magnitude gain in signal/noise ratio over resistive dividers.

4. Amplifier. For certain very low signal levels a high-gain, high-frequency amplifier is necessary. The Model 4366E wideband

amplifier was made by C-Cor Corporation. According to C-Cor it has an equivalent noise input of 40μ V and a 50 ohm input and output impedance. The 40 μV equivalent noise input is spread over a frequency range up to 200 MHz (i.e. the noise is 0.2μ V/MHz). In terms of the maximum IF bandwidth of a spectrum analyzer equal to 20 kHz, the noise becomes 0.01μ V. Here the noise is insignificant.

B. Particle Studies. Various types of particles were studied to give a better idea of the necessary particle properties. Metals (aluminum, steel, graphite, amorphous carbon), planar dielectrics (paper, plexiglas, glass beads, mycalex, white paint, and zinc orthosilicate), and volume scatterers (Teflon, polyethylene, and particles suspended in liquids and solids) were studied under various conditions. Several of the particle studies (graphite, amorphous carbon, glass beads, zinc orthosilicate, Teflon) were made using static systems. The basic arrangement is shown in Figure 1, where the components are as labeled. The motor was used only for dynamic studies. Since a primary factor to be considered in the selection of particles was the intensity of backscattered radiation and its spatial distribution in the back 2π steradians of space centered about the focal point, many of the initial studies were made by visual observation of the backscattered light characteristics. This permitted obtaining general information about several scattering systems. Those scatterers found suitable in these tests were then subjected to more rigorous tests. Since the particle size had been limited to those whose secondary radiation obeys Mie scattering theory, large flat particles and small (molecular)

size particles were eliminated from the experimental studies. After the scatterers had been thus selected, they were studied in more detail.

The preparation of the scattering surface depended upon the desired scattering characteristics and the dielectric and physical characteristics of the substrate material. Soft metallic scatterers (aluminum) were prepared by using SiC or by sandblasting the surface under conditions of different abrasive velocity, particulate size, blasting time, and nozzle-to-surface distance. Hard metals (steel) were conditioned with various grits of alumina or SiC rubbed on the surface in random directions. Rubbing the substrate in a single direction produced a reflective diffraction grating which oriented the backscattered light in a plane, leading to a low duty cycle, pulsed readout as the plane rotated about the incident optic axis.

The dielectrics as a rule required special treatment. Teflon and polyethylene, which are dependent scatterers because of their physical composition, required no special preparation other than removal of surface scratches to eliminate surface interference. Other volume scatterers were made of paint pigment suspended in silicone resin. The pigment was separated from highly reflective paint supplied by 3M Company. The silicone resins were two-component optical quality resins having greater than 90 percent transmission. They were Dow Corning XR-63-493 resin and General Electric RTV-615A resin.

Plexiglas was treated with various chemicals in which it is soluble. None of the surfaces were suitably uniform. Plexiglass was sandblasted to produce a surface closely analogous to a gaseous or liquid system with suspended particles. That is, the forward-to-backward scattering ratio could be varied to match that of various particle concentrations in a fluid system. White paint pigment supplied by 3M Company was applied to substrates in two different ways. First, the paint was simply applied as a liquid and permitted to dry. Secondly, the pigment was separated from its carrier and binders and applied to a polystyrene disc as a dry powder.

The flat surface of a graphite welding electrode was used as a scattering medium. It received no surface treatment. Amorphous carbon was suspended in a volatile liquid and allowed to deposit onto a substrate. Zinc orthosilicate powder was prepared in the same manner. Various grades of paper were attached to the surface of a disc and studied. A mycalex disc was prepared and studied under dynamic conditions. Glass beads were studied under static conditions and were not attached to a substrate.

C. Study of System Parameters Using Rotating Disc. A single basic system was used for this and subsequent studies. A modular concept was developed to permit easy exchange of components and removal or addition of components as the study demanded. Figure 2 shows this basic system. Changes in succeeding experiments will be referred back to this figure. The components are as labeled

in the drawing. The rotating disc was driven throughout most of the study by a 400 Hz alternating current motor. A Behlman-Invar Model 503A Invertron frequency generator was used after it was found that the speed of a regulated direct current motor was not stable enough. This arrangement provided an extremely stable disc rotational velocity which was reflected in a constant Doppler frequency shift.

The system optics were critical and evolved because of the necessity of maximum incident intensity upon the scattering medium. The mirrors were made by metal deposition upon an ultraclean optically flat glass substrate. First, an opaque coat of titanium was evaporated onto the glass surface to form a good glass-metal bond. Next, a thick film of gold was evaporated over the titanium. The freshly evaporated metals were exposed to an inert atmosphere until they had cooled. This procedure produced mirrors which reflected greater than 95 percent of the incident radiation at 6328 angstroms. This figure is very near the maximum value obtained for metallic films (9).

The beam splitter is a commercially available dual prism arrangement with internal metal reflectors. This beam splitter has the following salient values: absorption 8.9 percent, reflection 41.1 percent, and transmission 50 percent for one beam; and absorption 21.7 percent, reflection 28.3 percent, and transmission 50 percent for the other heterodyned beam. The modulation indices are 0.822 and 0.566 respectively for uniform beams.

The original lens used in the optical network for early experiments had a focal length of 8 inches and a diameter of 5 inches. These dimensions were ideally suitable for the studies, because of the small f/number and large sampling angle, θ. The f/number was determined by the 2 mm laser beam diameter, not by the lens diameter. However, the loss of light being transmitted through the lens was rather high because of the deterioration of the anti-reflective coatings and inhomogeneities in the lens (see Figure 3). A corrected lens from a Tropel 4-inch collimator with a focal length of 40 cm and a 10 cm diameter with high quality anti-reflective coatings was substituted in later studies (see Figure 4). It has a transmission of 92.9 percent. Figures 3 and 4 are effectively plots of the distortions across the radius of each lens.

For longitudinal mode studies a glass retarder was introduced into the shorter beam (leg number 2 in Figure 2) between the lens and the beam splitter. A mirror was sometimes introduced into the other two mixed beams emerging from the beam splitter to provide a larger light flux on the photocathode and a resultant signal increase.

D. Polarization Studies. A Spectra Physics Model 310 polarization rotator was the primary instrument used in the polarization studies. For studying the effect of orientation of incident $\vec{E}$ vector it was placed in the unmodified beam from the laser. Its transmittance was 95.5 percent and its extinction was 1000/1. It was placed in one of the legs of the heterodyne network (see Figure 2) for the studies of heterodyne efficiency as related to orientation

of the polarization ellipse produced by Mie scattering. For some of those studies polarizers were introduced into both legs of the heterodyne system. A Hewlett-Packard 425A voltmeter was used to read out the data from the photomultiplier. An aluminum disc was used in the metallic studies and a disc painted with 3M paint pigment was used in the dielectric studies. Various sizes of apertures were used in the study of individual lobes.

E. Studies of Solid Volume Scatterers. In the study of solid volume scatterers the discs used in previous experiments were replaced with volumes of the same diameter as the discs but with substantial depth. This volume was molded of optical quality silicone potting compounds with a homogeneous mixture of suspended 3M paint particles. The motor on which the scattering volume was mounted was placed on a sliding platform and was driven with a micrometer screw to provide accurate measurement of the location of the focus within the scattering volume. Some studies were made with the incident beam impinging upon the edge - rather than the flat surface - of the volume. In this case the motor was mounted with its axis in a vertical position. It was still moved along the optical axis which was then perpendicular to the motor axis.

F. Liquid Volume Scattering Studies. The motor arrangement was replaced with a flowing liquid system in which pigment particles were suspended. The chamber was made of one inch aluminum channel with square cross section. Two high quality microscope slides were mounted opposite each other in the center of the channel which

was long enough that the criteria for laminar flow could be fulfilled on either side of the windows. The particles were suspended in water and the dilute solution was pumped in a continuous cycle by a centrifugal pump. The velocity of the fluid was controlled by a valve located on the exit side of the pump. The expansion caused by temperature changes was compensated for by a capacitance located in the fluid line. Extreme care was taken to prevent air bubbles being introduced into the fluid, since their presence would affect the accuracy of the readout. Flexible tubing was used on both ends of the scattering chamber to minimize vibrations being transmitted into the optical network. The system was completely closed to prevent contamination and to help eliminate air bubbles.

V. EXPERIMENTAL AND THEORETICAL RESULTS

The results of the experimental and theoretical studies outlined previously did not frequently present concrete quantitative results. Much of the information was relative to information obtained from other systems. Therefore, long lists of data can not be included. However, the information obtained is of significant value in relation to understanding the behavior of the optical system and in the attempted optimization of this system.

The following sections contain the results obtained under various constraints imposed upon the system and discussed previously. The parameters studied within these broad constraints were related to the scattering particles, the basic experimental setup, variables that affected this basic setup, and the utilization of the results leading to a system with optimum characteristics.

A. Study of Scattering Centers (Experimental). The results of the study of various scattering particles and their interaction with optical radiation are presented in Table 4. Those scattering centers which were visually examined and eliminated early in the studies are rated relative to one another. Those which were more thoroughly studied have a signal-to-noise ratio specified in the table. The signal-to-noise ratios are small because of the low signal-to-noise ratios of the output beam of the 0.5 mW Perkin Elmer Model 5200 laser used in the studies.

B. Design of Basic Experimental Setup. Part of the purpose of this research was the evolution of a suitably optimized experimental

device which would serve as a basic element for devices for possible field use. Of course, a well planned and theoretically substantiated configuration was necessary in the beginning. This initial concept is shown in Figure 2. The result of the evolution depended upon the other studies and is included in Figure 14.

C. Alignment of the Heterodyned Beams. Misalignment of light rays within beams and misalignment of the beams themselves in a heterodyne system cause a rapid loss in heterodyne current. The causes of loss of heterodyne current related to the various possible misalignments are tabulated in Table 5. The information in Table 5 is in agreement with the theoretical treatment of Lee (10).

Coincidence of the two beams over 30 feet is necessary for alignment within 2 seconds of arc. A suitable compromise with distortions caused by the lens was determined to be between 15 and 20 feet.

D. Effect of Disc Velocity on Data. The stability of the velocity of the scattering particles played an important part in the accuracy of the readout. Rapidly changing velocity produced an effective broadening of the spectrum analyzer display; slow changes in velocity made it almost impossible to read the value of Doppler frequency from the spectrum analyzer display screen. With a highly stable frequency out of the power supply the velocity was constant, and the velocity calculated from experimental values of the Doppler frequency agreed with those from the known disc velocity.

E. Location of Limiting Apertures.(Effect of Variation in Observation Angle). The location of the limiting apertures in the backscattered radiation determine the magnitude of the observation angle and the observation plane. The percent error introduced by assuming the Doppler frequency to be linear with aperture position within certain geometrical limits is tabulated in Table 6.

F. Causes of Frequency Spread. Several factors were thought to possible have an effect upon the width of the Doppler frequency display on a spectrum analyzer. Both those that had no effect under the constraints imposed on particle size distribution, size, concentration and on system configuration and those that did have an effect under the given constraints were studied. Several were eliminated because of scattering particle characteristics, others were eliminated because of the symmetry of the heterodyne system. The results of the frequency spread studies are given in Table 7.

G. Isofrequency Lines. Contours of equal frequency existed on either side of a vertical line perpendicular to the optical plane and intersecting the major optical axis. These contours were symmetrical about this line. A plot of the isofrequency lines transversed by the normally used sampling points (corresponding to limiting apertures located approximately 6° on either side of the optical axis) is given in Figure 5 and tabulated in Table 8.

H. Frequency Measurement Limits. There were found to be several elements in the system which could limit the Doppler frequency and therefore limit the maximum and minimum particle velocities

which could be measured. Most of these limits did not affect the study of two- and three-dimensional scatterers or laminar flowing systems. However, the upper frequency limit of the Singer SPA-3/25a spectrum analyzer did limit the velocities under certain high frequency conditions. Of course, the lower limits of the Tektronix 1L10 and 1L20 spectrum analyzers did limit measurements on the low frequency end. The upper and lower frequency limits are not basic but depend upon the various electronic elements in the system. These limits are given in Table 9.

I. Noise. Several sources of noise were found to exist within the optical system. All contributed to the signal-to-noise and some were impossible to eliminate. The laser contributed most to the noise. Some incoherent sources such as ambient light were intolerable. The noise caused by electronic devices was minimal. The sources of noise with their magnitudes are given in Table 10.

J. Intensity and Signal-to-Noise Ratio. The signal-to-noise ratio as read on the CRT of the spectrum analyzer determines the minimum amount of heterodyne current which can be measured. If a large noise level is introduced by ambient light or by unheterodyned laser light, the signal may be attenuated to an extent that it cannot be resolved from the large amplitude noise. There were several sources of noise in the system which caused a resultant decrease in signal-to-noise ratio. The largest attenuation occurred at the scattering medium. The causes of low signal-to-noise ratio are tabulated in Table 11. The relationship between the photomultiplier characteristics and signal-to-noise ratio can be ascertained from Table 12.

K. Polarization Studies. The optical components contributed to the state of polarization of the radiation at different points in the system. The orientation of the incident $\vec{E}$ vector made no contribution to the data. The effect of the gold reflecting mirrors on the polarization of light is presented in Table 13 and Figure 6. The effects of the beam splitter on the polarization of both the transmitted and reflected beams are presented in Figure 7 and in Table 14. The effects of aperture diameter on the eccentricity of the polarization ellipse for a dynamic scattering medium are given in Table 15. The relationships between the scattering angle and the $\vec{E}$ vector orientation ϕ for maximum and minimum intensities and the ratio of major to minor axis for the polarization ellipse are given in Table 16.

L. Solid Volume Scatterers. The volume made of optical quality silicone resin with suspended particles from 3M Velvet Coating was studied to determine the additional effects caused by a three--dimensional scatterer. The concentration of particles was chosen to prevent both dependent and multiple scattering. When the scatterer was oriented so that the motor axis, velocity vector and incident light beam were mutually orthogonal, the depth of the sampling volume within the silicone resin was read out as a Doppler frequency on the spectrum analyzer. This frequency was linear with the depth of the focal point within the scattering volume. The scattered intensity varied from a maximum at the surface of the silicone resin interface with air, through a long flat plateau within the silicone resin, then to another maximum

at the interface of the silicone with a metal supporting cylinder mounted coaxially about the motor axis.

M. Liquid Volume Scatterers. The flowing liquid system was used to determine the additional effects of a flowing fluid upon the data obtained using two- and three-dimensional solid scatterers. Air bubbles suspended in the flowing stream produced such a low backscattering intensity that they could be ignored. The accurate measurement of data was hampered by the low velocity of a laminar fluid which positioned the Doppler frequency peak in the region of the longitudinal mode noise caused by the Spectra-Physics 125 laser. The width of the Doppler frequency line was less than the 50 kHz linewidth of the spectrum analyzer. The value of the Doppler frequency was approximately 250 kHz.

VI. DISCUSSION OF RESULTS

A. Study of Scattering Centers (Experimental). As can be seen from the theoretical discussion on page 10, the best light scatterers would be flat dielectric plates of low density and high polarizability oriented with their plane faces perpendicular to the incident radiation. These, of course, cannot be used because of their necessarily time-variant orientations in turbulent systems. The next best alternative appeared to be perfectly spherical dielectric particles of uniform size. Therefore, much of the experimental work has been oriented toward finding this type particle. However, these are not necessarily superior for experimental studies and as a result other systems were studied.

Since one of the primary goals of this study was to ascertain the variables which contribute to the readout, it proved necessary to develop an understanding of system parameters and anomalies in a logical manner.

The particular approach which was selected was to simulate possible particle systems in a well defined two-dimensional domain. This permitted a suppression of several variables which would be present in a three-dimensional turbulent gas or liquid system. This approach permitted an independent study of many of the parameters of the measuring system.

The experimental arrangement for measuring the characteristics of the scattering centers is shown in Figure 1. The amount of light scattered from the disc was measured at specific angles relative to the incident beam. The relative magnitudes of the

signal-to-noise ratios as developed by the scattered light were of greater interest. Because of the primary purpose of obtaining scattering centers which gave lobes that were rotated at preselected angles and which were of high intensity, precise quantitative data were not taken. Despite this, considerable effort was expended toward the selection of the appropriate surface. The results of this study are given in Table 4.

The study of these surfaces were based upon the necessity for knowing the following:

1. Effect of particle size on scattered light lobe shape, orientation, and intensity.
2. Effect of particle concentration on the above lobe qualities.
3. Effect of particle size distribution on the same qualities.
4. Effect of substrate condition on the above qualities.
5. Effect of methods of producing the particles on the above qualities.
6. Effect of the nature of the material of which the particles were formed upon their characteristics (color, shape, electrical conductivity, etc.).

The size, shape, distribution, and concentration of the different particles were determined using a shadowgraph and a 430 power microscope. The opaque substrates caused the normal forward scattering lobe to be folded back along and to either side of the incident beam.

In general the following methods of application or formation of particles were used:

1. Chemical treatment of soluble substrates — Approximately thirty chemical solvents were brushed, sprayed, or poured on clean plastics such as plexiglas or lucite. The most uniform results were obtained by pouring acrylonitrile over plexiglas. Bis (2-methyoxyethyl) ether and pyridine were roughly comparable. However, several problems were associated with this technique. The particle sizes were so small that the backscattering lobes were dim and distributed over a large solid angle, the particle concentration was so high that the scattering was dependent, and the uniformity of particle distribution was sufficiently poor to give a constantly changing signal-to-noise ratio as the disc was rotated. The signal-to-noise ratio varied from practically unity to about four-to-one. Additional applications of acrylonitrile helped the uniformity problem, but other considerations ruled out the use of this technique.

2. Bulk graphite — The flat surface of a graphite electrode was used as a scattering medium. In this case the graphite is a good absorber and the backscattered intensity is low. The graphite platelets which acted as scatterers deviated severely from the developed Mie theory, which considers only spheres.

3. Mechanical deposition of powder on substrate — Carbon black deposited on a substrate was rejected because it absorbed a great deal more incident light than graphite. Zinc orthosilicate

deposited easily, had particles in the desirable size region ($\approx 20\mu$), and absorbed little incident radiation. However, since the particles were not of uniform shape, and the scattering occurred over a large solid angle, it was not possible to orient the back scattered lobes at the desired angles.

4. Paper — Several grades of paper varying from high-quality tracing paper to rough cleaning tissue were used. The highest quality tracing paper presented particles of non-uniform size, distribution and shape. The resultant scattering from the surface was exceedingly random and the lobes could not be shaped. The scattering from the cleaning tissue was not intense enough to be seen. It can be speculated, however, that there was also a great deal of highly random scattering since the paper, when magnified, was extremely non-uniform with scattering centers more closely approximating cylinders than spheres.

5. Glass based discs — Mycalex, a solid mixture of mica and glass fragments, had a large amount of reflection. However, a great deal of scattering occurred below the surface causing the net scattering to be dependent. Films deposited on glass substrates and partially etched away were not successful because of the difficulty of standardizing the particle sizes, shapes, and distributions. The backscattered lobe was shaped well and was located coaxially about the incident beam.

6. Metal surfaces — Metal surfaces were usually prepared by sandblasting or sandpapering. The particle sizes were determined

by the size of the sandblasting particles or the grit of the sandpaper (SiC). The scattering from some of these surfaces was surprisingly independent as indicated by the minimal lobe interaction. This is probably because of the three-dimensional nature of the discs — as if the particles were suspended on a substrate whose reflected light originates from a plane sufficiently deep within the disc to not interfere with the desired scattering. The independence could be improved by applying more force to the sandblasting particles or to the sandpaper. The "smoothest" surface was prepared with crocus cloth and was completely unusable because of an almost matted finish causing a severe loss in intensity. The roughest surface was made with "pebble" size sandpaper and had purely diffuse scattering with low efficiency. Intermediate particles provided better scattering intensity and lobe distributions. The lobes could be shaped and rotated relatively easily by varying some of the parameters mentioned above. Of course, the ideal condition would be a large backscattered lobe envelope, elongated along and adjacent to the incident axis.

Obtaining uniform surfaces with either of these techniques was not difficult. In sandblasting, the distance from the point source of abrasive to the surface under preparation was the key to uniformity. In sandpapering, the biggest problem was to insure that the lines formed by the sandpaper were broken up into small segments. If this were not done, the radiation scattered from the lines produced a direction sensitive pattern. In this case a small angular segment contained the majority of the re-emitted

radiation and varied its spatial position as the disc was rotated. The resultant readout consisted of good data for a small portion of a cycle and no discernable data during the remainder of the cycle. This problem was eliminated by sanding the surface in a completely random manner. The scattered radiation was only slightly depolarized so that under many conditions the heterodyned signal was reduced because of an angle between the $\vec{E}$ vectors of the two heterodyned beams. Steel was the most efficient scatterer; aluminum was the least efficient when prepared by sandblasting. Aluminum prepared with sandpaper became the standard for future studies. The scattering centers on it possessed diameters of approximately 10 microns.

Dielectric surfaces were also prepared by sandblasting. It was not possible to use sandpaper or alumina because of the large amounts of abrasive material remaining in the surface. Dielectric surfaces prepared by sandblasting were good analogies to a laminar fluid flow carrying suspended scattering particles since the ratio of forward to backward lobe intensities was preserved. However, it was impossible to get good quantitative data from the backscattered lobes because of the low scattering intensity using the laser available at the time these studies were made. The particle sizes, densities, shapes and distributions were suitable. Surfaces prepared with available alumina powders were unsuitable, because they become attached to the surface making good absorbers.

7. Painted surfaces — The most effective scattering surfaces have been prepared by using a highly reflective enamel manufactured by the 3M Company (NEXEL Brand velvet coating No. 202-A10 white enamel). The particles of pigment in this enamel more closely approximate the spherical, uniform size, dielectric spheres described by Mie theory. The lobes from this paint cannot be shaped at will but the scattered intensity is sufficiently high to recommend the use of this scattering system over any of the others. The scattering properties are not significantly changed by mechanical contact and the particles can be used continuously at 160° F. Apparently, the absorption by the pigment is low and the scattered intensity is high and essentially uniform (except for the fine lobed structure inherent in scattering of coherent light) over 2π steradians. According to the manufacturer it "provides directional reflectance more uniform than a freshly sanded magnesium carbonate block..." (the optical reflectance standard).

It was possible to separate this pigment from its vehicle into a dry powder. This powder was applied to plexiglas surfaces to provide an analogy to a flowing stream with suspended scatterers. The forward-backward intensity ratio was consistent with that anticipated for particles of this size ($\approx 20\mu$). In fact, the pigment was sufficiently efficient as a scattering medium to use it as the contaminant in a recirculating laminar or turbulent fluid stream. The cost was small enough to permit its use for

this purpose but the separation process was not efficient enough nor the cost small enough to permit the use of the pigment in systems that do not recirculate.

The pigment was more efficient for backscattering than other commonly mentioned scattering particles, having a scattering efficiency greater than 85 percent. Water has a low refractive index and is transparent; therefore, it transmits an appreciable amount of light. Spherical glass beads and plastic spheres are readily available but suffer from a higher transmittance. An additional problem with any transparent particle concerns its two surfaces.

A transparent spherical particle may be considered as a short focal length lens with a highly curved mirror placed in series. Light incident upon the first surface is scattered. Then some light is transmitted to the second surface where it is again scattered. The two backscattered waves present two wavefronts to the readout device. In addition, appreciable interference occurs between the two wavefronts. Therefore, the intensity of radiation scattered from transparent particles is reduced not only by the more efficient transmission but also by the interaction between the two surfaces of the sphere (dependent scattering). Nonspherical particles introduce more complex considerations.

Carbon particles, as mentioned before, absorb light and are thus more inefficient as scatterers than the pigment.

Studies were made on volume scatterers. The available scatterers were polymers and did not give independent scattering.

Bulk Teflon (which is thought to be a combination of amorphous and crystalline material) and polyethylene were used. Their dependent, multiple scattering was immediately obvious since the entire disc became a secondary emitter of the incident radiation. Volume scatterers made of silicone and 3M pigment will be discussed in a later section.

All of the dielectric particles mentioned above scatter any incident radiation as elliptically polarized light. The metals preserve the polarization condition of the incident light. Each of the small lobes making up a large lobe consists of slightly different degrees of elliptical polarization. Therefore, the size of the readout apertures are important in optimum matching of polarization vectors. However, the size of the aperture is more important in its own right above certain small diameters, since doubling the area of the aperture doubles the signal. However, as a maximum, it is only possible to approach doubling the signal by matching polarization vectors.

B. Design of Basic Experimental Setup. Since the configuration used in this study differs considerably from previously used arrangements, reasons for its selection will be discussed. The backscattered configuration was initially chosen because of the desirability, and indeed the necessity, of using it in its ultimate application of determination of the flow about the base of a rocket. The symmetric, dual scattered beam heterodyne configuration (see Figure 2) was chosen because of the inherent ability

of the arrangement to cancel the frequency spread because of the finite width of the limiting apertures (16) and to compensate for changes in modulation index caused by time variant scattering intensity. By using the symmetric configuration the effective Doppler frequency shift is approximately doubled, and the spread in this range of frequencies is that possessed by an aperture approaching zero diameter.

If a single scattered beam were beat with the unshifted incident beam as was done in previously described systems, the frequency spread would be a linear function (at small observation angles) of the aperture diameter. This measurement was made by scanning a slit across the beams perpendicular to their axes. This can be seen by considering the equation relating the frequency of the Doppler shift to the angle of incident radiation relative to the velocity vector and the observation angle relative to the incident beam:

$$f_D = \frac{2 V_n}{\lambda'} \sin\frac{\theta}{2} \left(\psi + \frac{\theta}{2}\right) \qquad (14)$$

where V_n = velocity along a given axis of a coordinate system centered at the focal point

λ' = vacuum wavelength of the incident radiation (6328 Å for a He-Ne laser)

θ = observation angle relative to incident radiation

ψ = angle between the velocity component and the incident radiation

f_D = magnitude of the Doppler frequency shift.

For a system in which $\Psi = \pi/2$ and the incident radiation can be approximated as having no beam size or convergence angle, the equation becomes simply

$$f_D = \frac{v_n}{\lambda'} \sin \theta. \tag{15}$$

For calculating the center frequency at which the Doppler shifts occur, this approximation becomes exact.

Optical filters must be introduced in the incident beam to attenuate the amplitude to a value equal to that of the single scattered beam. The filters introduce interference fringes which cause an increase in noise and a resultant decrease in signal-to-noise ratio. The uniform radiation pattern of the incident beam mixed with the lobed structure of the scattered beam also contributed to the deterioration in signal-to-noise ratio.

The symmetric heterodyne techniques chosen for this study eliminates many of the problems of the single heterodyne technique. Here it is necessary to modify equations 14 and 15 to compensate for heterodyning occurring as a result of mixing two Doppler shifted beams together rather than mixing one shifted beam with the unshifted incident radiation. The three-dimensional equation was derived by Dodd (5)

$$\begin{aligned} f_{yz} &= 2/\lambda'(v_z \cos\alpha_{yz} + v_y \sin\alpha_{yz}) \sin\theta \\ f_{zx} &= 2/\lambda'(v_x \cos\alpha_{zx} + v_z \sin\alpha_{zx}) \sin\theta \\ f_{xy} &= 2/\lambda'(v_y \cos\alpha_{xy} + v_x \sin\alpha_{xy}) \sin\theta \end{aligned} \tag{16}$$

where the double subscripts indicate the plane in which the readout was taken and the single subscripts indicate the axis on

which the velocity vector was projected. The angle between any one of the cartesian axes and the velocity vector in a given plane is α_{mn}. The total angle of observation, θ, is taken between the two heterodyned beams.

For the symmetric system under consideration f_{zx}, f_{xy}, and α_{yz} are zero so that the Doppler frequency becomes

$$f_d = f_{yz} = \frac{2v_z}{\lambda'} \sin \theta \qquad (17)$$

which is exactly twice the value of a single sided heterodyne system as given in equation (15). Equation (16) must be used for a system in which α_{mn} is present.

The initial reason for choosing the symmetric configuration was to take advantage of doubling the Doppler frequency shift. This immediately permited ignoring some perturbations that occur at low frequencies - laser mode noise, mechanical vibrations, relatively low frequency electrical pickup, etc. In addition, within a given spectrum analyzer dispersion, a higher center frequency permits a lower error relative to the center frequency. The error caused by the uncertainty of readout is constant with dispersion for a linear dispersion scale.

Additional problems occur when a scattered beam is heterodyned with a beam taken from the incident beam or from the rear of the laser as was done in several experiments. The non-scattered beam is inherently more intense than the scattered beam. In the process of attenuating the beam to be more nearly equal to that of the scattered beam, interference fringes are introduced which lower the overall intensity (heterodyne current). In addition, the system becomes

vibration sensitive because of the movement of the interference fringes.

The initial design results are shown in Figure 2. The plane polarized light from a Perkin Elmer 5200 laser with an output of 0.5 mW impinged, after passing through several spatial filters, upon a 5 inch lens (not highly corrected, see Figure 3) which focused the beam upon a rotating disc. The focal length of the lens was approximately 8 inches. The rotating disc was mounted on a high speed D.C. aircraft pump motor which was powered by a series of wet cell D.C. batteries. The incident beam was focused on the vertical axis of the disc and approximately 1.0 inch above the horizontal axis. The vertical axis was chosen to give symmetry of the isofrequency lines about the incident beam. The distance from the horizontal axis was not critical and was variable. However, as will be seen later, the frequency spread decreased as this distance increased. Variation of this distance affected the frequency of the scattered radiation in a linear manner.

Determination of the exact location of the focal point was difficult. The best procedure suffered from the aberrations introduced into the back scattered beam by the lens. However, it was used in lieu of any more precise method. First, the limiting apertures and beam splitter were removed and the scattered light through one half of the lens was allowed to impinge upon a mirror, which reflected the beam over a distance

of about fifteen feet. A large aperture, or a matrix of small apertures, was placed in the beam near the mirror. At the terminus of the beam a replica of the aperture or matrix was placed in the beam. The lens position was then varied along the optical axis until the beams defined by the first aperture or matrix coincided with the duplicate at the other end of the beam. A large aperture or several small ones were chosen to minimize the uncertainty caused by diffraction at the edges of all apertures. A distance longer than fifteen feet would have been preferable except for the barrel distortion of the lens. The location of the focal point could be roughly determined by placing the disc in the focused beam and filtering out the coherent red light normally scattered into the eyes. The blue light which remains is focused to a much less intense spot near the focus for the red light. The position of the disc along the optic axis is then adjusted until the blue spot is of minimum size.

It was also important that the disc be perpendicular to the optical axis in order to maintain the symmetry of the device. Otherwise the value of α would not be zero.

The radiation was scattered from a point on the disc according to the conditions of the particles on the disc as discussed above. All of the rays that were backscattered through the lens were made parallel again (within limits of the correction of the lens). Two segments on the horizontal axis spaced symmetrically about the incident beam were intercepted by circular

apertures, forming pencil beams. The distance from the apertures to the incident beam was variable. Variation of these distances changed the observation angle, θ, which resulted in a change in the value of the frequency of scattered radiation.

The two cylindrical beams were intercepted by a mirror and a beam splitter respectively and brought together on the face of a DuMont 6911 photomultiplier whose output was read on the cathode ray tube of a Singer Panoramic SPA-3/25a spectrum analyzer.

Utilizing this basic setup, some of the experiments carried out and some problems that arose can be discussed. The primary experimental goal was to determine what parameters contributed to the data and to build a solid basis for studies of turbulent flow.

C. Alignment of the Heterodyned Beams. One of the most difficult early problems was the alignment of the beams to an accuracy sufficient to get a useable signal-to-noise ratio. Part of the problem was a naive idea of the criteria necessary to produce maximum heterodyne current at the output of the photomultiplier. Through a tedious manipulation of variables, an overall view of the necessary cirteria began to unfold. Later, after an unpublished report by Lee (10) became available, the close agreement between the experimentally determined criteria and those predicted by Lee was encouraging. The facotrs which were found to affect the quantity of heterodyne current are given in Table 5.

An additional consideration predicted by Lee that was not seen experimentally in this apparatus concerned the size of the photomultiplier aperture, which in this case was determined by the 0.154 inch diameter of each of the defining apertures in the backscattered beam. In the process of another experiment, apertures larger than one inch in diameter were used with no apparent reduction in the extrapolated heterodyne current because of loss of spatial coherence at the large aperture.

It experimentally was determined that a distance of at least 15 to 20 feet was necessary as a lever arm to suitably align the two beams. That is, if within the ability of the eye to resolve, the beams were made coterminous over a distance of greater than fifteen feet, the heterodyned current was optimized as to angular and spatial separation. Theoretically, the larger the lever arm the more accurate would be the alignment and the higher the heterodyne current. However, because of a barrel distortion in the lens, any larger distance of alignment introduced an uncertainty which usually led to reduced heterodyne current.

The condition that the two beams coincide both vertically and horizontally at the beam splitter was of special importance. This criterion was frequently hard to meet because of obvious observation problems. There were two procedures that were mutually complementary in determining whether the beams were sufficiently coaxial. First, with the disc stationary the two beams were "walked" as nearly as possible into coincidence. In this case the natural room vibrations became important. If the two beams were

completely coincident there would be a low frequency flicker of the net beam intensity as the phase differences of the two beams alternately attempted to cancel and complement each other. This case was analogous to the case of two coincident non-scattered beams which could be made to completely cancel (180^{o} out of phase) or complement each other — in the first case effectively cutting off the laser, in the second case doubling the amplitude of the beam. As the beams deviated from coincidence, the interference was an angular effect causing the transition from no fringes (at coincidence) to large numbers at relatively small angles of separation. Since interference no longer was angle independent, it was not complete over a long linear segment of the beams. Therefore, the positioning of the photomultiplier became critical and the system was vibration sensitive. An alternative was to look at the low frequency Doppler signal on an oscilloscope, and adjust it to maximum. This was impractical with the spectrum analyzer. Obviously it was desirable to have the light spread over as much of the interfering beams as possible. A technique that was felt would help compensate for misalignment was to focus the beams onto the surface of the photocathode. This would make all rays parallel at the focal point. This technique was soon discontinued because of the sensitivity to vibration as the photocathode mechanically oscillated about the focal point, and because of a reduction in heterodyne current due to losses at the lens. Later, the basic concept of focusing the heterodyned beams was found to have been

predicted by Lee. In theory the concept was good; in practice it was so difficult to implement that it was not worth the effort, as was experimentally determined.

The second check on the beam alignment (which incidentally checked the difference in parallelism of rays within the two beams) was performed with the disc rotating. The rotating disc integrated the mottled appearance of each of the two scattered beams into two uniform light discs with well-defined edges. Over the distance of fifteen feet the edges of the beams could be made coincident to a high degree of accuracy. It was not possible to use an oscilloscope to align this high frequency Doppler signal. The peak could be maximized using a spectrum analyzer, but this technique was difficult. Experimental evidence indicated that by properly utilizing these suggested alignment techniques, the heterodyne current was maximized.

It was also important to have the components affecting the incident beam coaxial to the beam. If this condition is not met, the spatial filters would decrease the radiation intensity. If the lens was not centered on the incident beam, the resultant scattering was skewed. These criteria were met by reflecting the light until it re-entered the laser.

D. Effect of Disc Velocity on Data. A variable velocity scattering medium was used to permit simulation of the different velocities that had been used by Foreman, et al. (6) in their laminar flow measurements. For a reasonably compact system with disc radius R = 2.5 inches this would require a motor speed

of 0.75 rpm to 43,545 rpm, corresponding to gas velocities from 0.5 to 28,954 cm/sec. In a 0.5 cm diameter tube, turbulence occurs for air according to

$$v = \frac{Rn}{D\rho} = 362 \text{ cm/sec} \qquad (18)$$

where $\rho = 1.213 \times 10^{-3}$ gm/cm^3 = density of air

$\eta = 1.827 \times 10^{-4}$ gm/sec cm = viscosity

$D = 0.5$ cm = tube diameter

$R = 1200$ = Reynolds number for turbulent flow.

The D.C. motor mentioned above had a capability of about 100 rpm to greater than 13,500 rpm with appreciable velocity variation — as much as 10 percent at midrange, more at low velocities. Because of severe vibrational problems at higher speeds, its practical use was limited to rather short periods because of component misalignment. This motor, powered by D.C. batteries, was sufficient for the intensity measurements described above. However, later measurements depended on a more stable center frequency for the measurement of this center frequency as well as the width of the display (frequency spread) on the spectrum analyzer. An attempt was made to use a unijunction-SCR D.C. motor regulator designed by General Electric. This regulator was supposed to be continuously variable in output voltage and as a result would give the motor a highly regulated continuously variable velocity. The regulator proved to be neither continuous nor a regulator at most frequencies.

In the earlier studies without the regulator and at the incremental frequencies at which the regulator would work, it was noted that the velocity of the motor had no measurable effect (other than the linear effect postulated by the Doppler equation) on the frequency spread or on the center frequency. Of course, at velocities at which mechanical vibrations become large, there is an effect caused by the misalignment of the system.

As a result of the above conclusion, it was decided to use a synchronous motor driven by a variable (280-520 Hz) frequency generator which had a frequency accuracy of 0.5 percent and a temperature coefficient of $\pm$ 0.01 percent/^{o}C. This permitted a motor speed of about 8380-15,570 rpm which was acceptable. Any shift in center frequency was too small to be measured or observed.

All of the measured values of frequency shift agreed with those predicted by the Doppler equation which was also checked. This, of course, was not true until the uncertainties in velocity were removed. This depended upon accurate measurement of θ, α, and the velocity of the disc.

E. Location of Limiting Apertures. (Angular) It was noted before that the limiting apertures were located symmetrically ontthe horizontal axis and on either side of the incident beam. Since the focal length of the lens was fixed, the position of the apertures uniquely determined the magnitude of the observation angle. In the early experiments the lens in use had a focal length of $\approx$8.0 inches and the apertures were spaced to give an observation angle of 6.0^{o} on either side of the incident beam. At an equivalent velocity of 880 cm/sec

(2800 rpm with R = 3 cm) this gave a total Doppler shift of

$$f_D = 2.9 \text{ MHz}$$

from equation (17). This value is approximately linearly related to higher or lower values of frequency as long as θ remains small. For example, the deviation of sin θ from θ at 15° is only 1.15 percent. This error becomes 0.15 percent at 6°.

Under conditions of small θ and $\alpha \approx 0^\circ$ the following approximations may be made

$$v_z \cos \alpha_{yz} + v_y \sin \alpha_{yz} \approx v_z$$

and

$$\sin \theta \approx \theta \tag{19}$$

Now, the Doppler equation reduces to

$$f_D \approx \frac{2 v_z \theta}{\lambda} \tag{20}$$

such that the value of f_D is effectively a linear function of the observation angle.

The variations of f_D from a linear function within the limiting angles defined by the lens aperture are shown in Table 6.

These values were calculated at a velocity of 2,905 cm/sec, which is an acceptable value for turbulence and was obtained easily with a rotating disc. The maximum observation angle subtended by the 5 inch lens was 17° 20'. Therefore, the maximum possible error using the edge of the lens as a limit was 1.54 percent. That is, for practical considerations the position of the apertures had no significant effect on the linearity of f_D.

The angle 6° 32' defined the limiting angle of the framework of the corrected 4 inch lens. As an indication of the total

accuracy of the system in relation to calculated and measured values of f_D, consider the 6° 32' angle and the 5° 31' angles, representing the range of errors. In the first case the measured value of f_D was 10.4593 MHz, the calculated value was 10.4471 MHz giving an error of approximately 0.12 percent. In the second case the measured value of f_D was 8.8599 MHz, the calculated value was 8.8274 MHz giving an error of approximately 0.37 percent. Both of these values are well within experimental error. If the two apertures had not been equallyspaced, however, error would have been introduced from several sources. First, the system would no longer by symmetrical, introducing a spread in frequency because of the non-superposition of the correct rays coming through the apertures. In addition, there would be a shift in the center frequency for the same reason. This would also invalidate the simple assumption that $\alpha = 0$, thereby complicating calculations.

The experimental determination agreed completely with the calculated values. The equality of the angles was checked by beating each backscattered beam with an unshifted beam. The center frequency of the two beams agreed, indicating that both sampling angles were equal.

F. Causes of Frequency Spread. The peak, as displayed on the spectrum analyzer, had a finite width. Since it was proposed to use the probability distribution function on the spectrum analyzer to study the turbulent flow of a fluid process, it was necessary to fully understand the causes if possible. This understanding was

crucial to the use of the heterodyne technique for determination of the characteristics of turbulent flow. If it were not possible to eliminate the causes they would have to be considered quantitatively in the data.

This degree of contribution of external effects and system parameters to the width of the frequency spectrum had to be known because of the time variant characteristics of turbulent flow. In other words, the time variant nature of turbulent flow produces a frequency spread of its own. It was postulated that the characteristics of this spread would be used to determine the characteristics of turbulent flow. If external effects also existed, producing a distribution of their own, the desired distribution would be modified or eliminated.

The classification of the possible causes of frequency spread fell into two classes: 1. Those that were postulated but did not contribute to the spread within the chosen constraints of particle size, size distribution, and concentration, and 2. Those that contributed significantly to the spread of Doppler frequencies.

1. Parameters which Did Not Contribute to Frequency Spread.

(1) Limiting Aperture Size – In systems utilizing heterodyning between a beam with no Doppler frequency shift and a Doppler frequency shifted beam, the spread in Doppler frequency is a sine function of the aperture size as derived from equation (14)

$$\Delta f_D = \frac{2v}{\lambda'}\left[\sin\frac{\theta_1}{2}\sin\left(\psi+\frac{\theta_1}{2}\right) - \sin\frac{\theta_2}{2}\sin\left(\psi+\frac{\theta_2}{2}\right)\right] \quad (21)$$

$$= \frac{v}{\lambda'}\sin\theta_1 - \sin\theta_2 \quad \text{if } \psi = \frac{\pi}{2}. \quad (22)$$

If θ_1 and θ_2 are small the relationship becomes linear

$$\Delta f_D = \frac{v}{\lambda'} (\theta_1 - \theta_2). \tag{23}$$

Here Δf_D is the spread in frequencies and θ_1 and θ_2 are the observation angles defined by the inner and outer edges of the limiting apertures respectively. This was checked experimentally by scanning a slit across the mixed beam resulting from combining a scattered beam with a direct beam of about the same size and intensity. The resultant plot of frequency versus distance is effectively linear.

On the other hand, when the mixed beams were both scattered in the perfectly symmetric manner described above and shown in more detail in Figure 9, the resultant frequency spread was zero. Since only the difference frequency is seen by the photomultiplier, the frequency distribution at the apertures is that given in Table 17. It can clearly be seen that the top beam is inverted such that the following differences hold:

$$\begin{aligned} f_C &= (f + 2\delta f) - (f - 2\delta f) = 4\delta f \\ f_T &= (f + 3\delta f) - (f - \delta f) = 4\delta f \\ f_B &= (f + \delta f) - (f - 3\delta f) = 4\delta f \end{aligned} \tag{24}$$

which is exactly twice the Doppler shift at the center of either aperture. Therefore,

$$\Delta f = f_C - f_T = f_T - f_B = \ldots = 0 \tag{25}$$

and there should be no frequency spread. This was checked by using larger apertures and by scanning a slit across the beam. Both techniques gave the same result: $\Delta f = 0$. For this to be

true the two apertures had to be accurately spaced and the two beams had to be coterminous.

(2) Particle Size - There was no frequency spread caused by particle sizes which were studied, since the Doppler frequency was a function of velocity of the particles and the particles were in a fixed matrix giving only one particle velocity. The small pigment particles supplied by 3M Company did not produce a measurable frequency spread in the flowing liquid system.

(3) Particle Size Distribution - Since the distribution of particle sizes was small (because uniformly sized Mie particles were being considered) the resultant velocity distributions were small. Approximately the same force was acting on all particles and the resultant spread in Doppler frequencies was small except at very low velocities where the distribution of velocities became significant in relation to the mean velocity (translational motion of the molecules). This latter value is insignficant for this high velocity study. Those particles held in a fixed matrix had no velocity distribution even when there was a size distribution.

(4) Distribution Caused by Variations in Motor Velocity - Formerly this gave a significant spread as the center frequency varied up and down the frequency scale. By using a synchronous motor the speed was constant so that a variation could not be measured with available equipment. Therefore, this contribution to the frequency spread was negligible.

(5) Movement of the Disc Parallel to the Incident Radiation (caused by bent shaft, disc of nonuniform thickness, deviation of disc from perpendicularity to beam, or warped disc) — This would effectively change the size of the beam continuously during a rotation and would result in changing scattered intensity and in a spread because of the beam size (see section below). The contribution to frequency spread due to these causes was easily minimized and as a result was not considered.

(6) Another source of Doppler frequency spread that is eliminated in the symmetric heterodyne configuration is that caused by convergence of the incident beam. Consider Figure 10, which is a representation of a single heterodyne system showing the focused beam converging onto a scattering plane moving with velocity, $\vec{v}$. The size of the beam entering the front surface of the lens is 2 mm in diameter to the 1/e power points. The focal length of the lens is 400 mm. Assume for the present that all rays from the incident beam coincide at a single point in the scattering plane. The half angle is defined as $\phi/2 = \tan^{-1} 1/400 \approx 10$ minutes of arc. This indicates the presence of two extreme conditions defining a maximum and a minimum Doppler shift. Consider the observation angle, θ, to be defined as the angle between the center of one limiting aperture and one of two rays defining the convergence angle of the incident beam. The value of Ψ is defined as the angle between $\vec{v}$ and one of the two rays defining the convergence angle. Under ideal assumptions ($\phi = 0$) $\Psi = 90^\circ$ and $\theta = 6^\circ$.

However, if $\phi \neq 0$ the values of ψ and θ deviate, introducing different Doppler frequency values. The important values are given in Table 18 where v_n = 632.8 cm/sec. The frequency difference

$$f_D = \frac{2v_n}{\lambda'} \left[\sin \frac{\theta_{max}}{2} \sin\left(\psi \max + \frac{\theta_{max}}{2}\right) - \sin \frac{\theta_{min}}{2} \sin\left(\psi \min - \frac{\theta_{min}}{2}\right) \right] \quad (26)$$

$$= f_D \text{ (max)} - f_D \text{ (min)} = 57.6 \text{ kHz} \quad (27)$$

was the spread of frequencies introduced into the signal by the convergency angle and was 5.51 percent of the center frequency and a linear function of velocity. The entire Doppler equation for a single beam heterodyne system must be used here since $\psi \neq \pi/2$.

It was not possible to measure this Doppler frequency spread directly because of the contribution of other factors. Instead, an indirect measurement was made using an optical collimator to increase the diameter of the beam from 2 mm (Gaussian 1/e power points) to a 50 mm (rectangular intensity cross section) incident beam.

Making the same calculations as before,

$$\varphi/2 \approx 3^\circ\ 30'$$

and Table 19 gives the parametric values. The data in Table 19 gives a Δf_D of 1.2 MHz for a calculated value. The approximate measured width was 1.0 MHz. This was low for three reasons: uncertainty in measuremant of width because of flattened display, decrease in vertical spot size, and decrease in horizontal spot

size because of diffraction limit decrease. This clearly indicates the deleterious effects large beam convergence can cause in a single beam heterodyne system.

On the other hand it can be seen from equation (16) that the Doppler frequency shift is independent of the angle of the incident beam in a symmetric heterodyne system. Therefore, a significant decrease in spectral line width on the spectrum analyzer is achieved.

2. Factors which Contributed to the Frequency Spread.

a. Spectrum Analyzer. A spectrum analyzer has a certain inherent peak width in its display of a function. If a line frequency of $f \pm 0.0$ were displayed on any spectrum analyzer it would be read as $f \pm \frac{\Delta f}{2}$, where Δf is the total frequency spread. This spread is a function of the video filtering, the sweep rate and the sweep width, but is primarily a function of the IF bandwidth of the spectrum analyzer. Because of its dependence on the IF bandwidth, it is of primary importance to have a maximum signal-to-noise ratio. This problem will be discussed in more detail later.

Before any meaningful studies could be made on the width of the frequency spread caused by the remainder of the system, it was necessary to substitute a Spectra Physics Model 125 laser with an output of greater than 50 mW for the 0.8 mW laser so that the signal-to-noise ratio could be increased. This change permitted measurement of the frequency spread caused by other effects. The Tektronix Model 1L10 spectrum analyzer has a low frequency-spread

limit and could be used in a certain frequency region to study the other effects discussed below. Ironically, its sweep width was so narrow that the effects of sampling volume prevented the use of the 1L10 on most system arrangements.

The Singer spectrum analyzer was used to take most of the data. Its dispersion, sweep rate, and IF bandwidth were adjusted to give maximum signal intensity. The width of the Doppler signal using the 0.8 mW laser was approximately 65 kHz with a signal-to-noise ratio of 4-to-1 under these conditions and when one backscattered beam was heterodyned with an unshifted beam. When both backscattered beams were heterodyned, the width was limited by the 50 kHz of the Singer spectrum analyzer.

The characteristics of the three spectrum analyzers which were employed are given in Table 2. These values were measured at half peak height. Generally the value is increased by a factor of two at 5 percent of total peak height.

The sweep rate was a major problem with the Tektronix spectrum analyzers. At low sweep rates the resolution was maintained but phosphorescence of the CRT screen was too short to study the display well; at higher sweep rates where the CRT display was acceptable the resolution and, therefore, peak amplitude deteriorated. Other speed CRT's are available.

b. Vertical Dimension of Scattering Area. The size of both the vertical and horizontal dimensions of the focused spot are limited by diffraction laws. The theoretical spot size which is produced by an aplanatic lens with f/number of unity cannot be obtained

without sacrificing other desirable characteristics. The aperture of an optical system through which a laser beam passes is defined by the diameter of the laser beam and not by the lens diameter. Therefore, the f/4 lens of this optical system becomes effectively an f/200 lens because of the 2mm diameter of the incident laser beam. Conversely, if a lens were chosen to give f/1 so that diffraction limited focus would be obtained, the focal length would be 2mm, creating a serious engineering problem. In addition, the incident convergence angle increases from approximately 20 minutes of arc to greater than 53 degrees, which distributes the frequency spread over a wide range in a single beam heterodyne configuration.

The absolute minimum spot size for a Gaussian beam with aperture f/1 and plane polarization is given as an ellipse with major axis $1.5\ \lambda/\pi$ and minor axis λ/π . This corresponds to the 1/e power points which comprise 63.2 percent of the beam power. The elliptical shape is caused by the oscillating dipoles which radiate more strongly along one axis than the other (14).

As the f/number increases from f/1 the significance of the theoretical limit becomes less important. The diameter of the diffraction limited focal point for an aplanatic lens would generally be the minimum spot size times the ratio of focal length to beam diameter. The length of the axes of the focal ellipse then become

$$\frac{1.5}{\pi} \cdot \frac{f}{d} \quad \text{and} \quad \frac{\lambda}{\pi} \cdot \frac{f}{d} \tag{28}$$

where d is the aperture diameter (laser beam diameter). This increases the minimum beam size by a factor of 200 for the system considered above.

For λ = 6328 Å the ellipsoidal dimensions are approximately 60 μby 40μ . The corresponding null-to-null diameter (Airy disc, containing 81 percent of power) of the usual circular diffraction pattern using unpolarized light is given by Carlin (3) as

$$\frac{3.83\lambda}{\pi} \cdot \frac{f}{d} = 153\mu. \qquad (29)$$

This is a more realistic value to be considered for the actual case because scattering prior to reaching the focal point, divergence of the laser beam, and the entire beam (as opposed to the 1/e power point) must be considered. The figure agrees roughly with that obtained from actual measurements. The value obtained by measurement was taken at other than the 1/e power point and extrapolated along the normal distribution curve to be about 261 μ. The corresponding Airy disc diameter was 276.6μ . Direct measurement was not possible because of the unavailability of appropriate apertures.

This value for the Airy disc will be used in the following calculations as a form of worst case analysis. The vertical dimension of the focused spot contributes to the Doppler frequency spread because of the possibility that it will contain several velocities. This is analogous to the scattering volume problem. The two-dimensional case is simple and demonstrates what effect

velocity distribution plays in signal spread.

Consider a perfectly parallel incident beam of diameter $d = 276.6\mu$ corresponding th the focal spot size discussed above (Figure 11). In this case, the light scattered from the top of the spot (where the disc velocity is higher) will be at a higher frequency than the light scattered from the bottom portion of the spot. Since the angles Θ and α can be assumed to be unaffected without loss of generality, the simple form of the Doppler equation can be used:

$$f_D = \frac{v_n}{\lambda'} \sin \Theta. \tag{30}$$

Now

$$\Delta f_D = f_D\,(\max) - f_D\,(\min) = \frac{\sin \Theta}{\lambda'} (v_{max} - v_{min}). \tag{31}$$

But by writing v_n in terms of the disc radii under consideration, the equation becomes

$$\Delta f_D = \frac{v_n}{R\lambda'} \sin \Theta\,(R_{max} - R_{min}) = \frac{v}{R\lambda'} \sin \Theta \Delta R \tag{32}$$

where Δf_D = frequency spread

v_n = mean radius of the disc = 2.324 cm

ΔR = spot size = 276.6μ = 0.02766 cm.

The quantity f_D can be calculated to be

$$\Delta f_D = \frac{(632.8)\ (\sin 6^\circ)\ (0.02766)}{(0.915)\ (2.54)\ (6.328 \times 10^{-5})} \tag{33}$$

$$\Delta f_D = \frac{(632.8)\ (0.10453)\ (0.02766)}{(0.915)\ (2.54)\ (6.328 \times 10^{-5})} \tag{34}$$

$$\Delta f_D = 12.42 \text{ kHz}.$$

The values of v, R, λ', and Θ will be constant for a given system and the frequency spread can be directly related to the

spot size by considering the following (16)

$$f_D = \frac{v_n}{\lambda'} \sin\theta = \left(\frac{2\pi f}{60\lambda}\right) R \sin\theta \tag{35}$$

$$\Delta f_D = \frac{2\pi f}{60\lambda'} \sin\theta \Delta R. \tag{36}$$

By dividing the first equation by the second a direct ratio is established:

$$\frac{f_D}{\Delta f_D} = \frac{R}{\Delta R}, \tag{37}$$

which indicates that the frequency spread is a direct function of the vertical spot size. In the above equation f is the motor speed in revolutions per minute. A calculation of Δf_D using this equation agrees with the above calculated value

$$\Delta f_D = \frac{f_D}{(R/R)} = \frac{1.045 \text{ MHz}}{(2.54 \times 0.915)/(0.02766)} = 12.43 \text{ kHz}. \tag{38}$$

c. Horizontal Dimension of Scattering Area. The other orthogonal dimension of the focused spot contributes nothing to the frequency spread as far as direct velocity variations are concerned. However, the effective observation angle is changed by the finite horizontal dimension of the spot, as shown in Figure 12. Of course, the leading and lagging edges of the focused spot are not at exactly the same radius as the center of the spot but, because of the small spot dimension, the value of ΔR is small enough to be negligible in the considerations in this case. Because the effect discussed here is simply a function of spot size the simple equation can again be used.

$$f_D = \frac{v}{\lambda'} \sin\theta \tag{39}$$

which becomes

$$\Delta f_D = \frac{v}{\lambda'} (\sin \theta_1 - \sin \theta_2) \qquad (40)$$

where θ_1 defines the angle between the normal and the lagging edge of the spot and θ_2 defines the angle between the normal and the leading edge of the spot. By construction of the parallel line h_2, it can be seen that the contribution of horizontal spot size is the same as for aperture contribution when a single scattered beam is mixed with an unscattered beam.

In terms of the geometry of the system this equation becomes

$$\Delta f_D = \frac{v_n}{\lambda'} \Delta(\sin \theta) = \frac{v}{\lambda'} \left(\frac{a}{\sqrt{f^2 + a^2}} - \frac{a - x}{\sqrt{f^2 + (a-x)^2}} \right) \qquad (41)$$

where a = the distance from the optical axis to the outer terminus of a limiting aperture

x = horizontal spot size

f = lens focal length = 40 cm.

This value of frequency spread, which for a symmetrical heterodyne system is the same at the external edge of each limiting aperture, is random in space and is not cancelled out by the beam overlapping. Since the value of $\theta \approx \sin \theta$ for small values of θ, the value of Δf_D is practically constant over rather large values of θ. for example, with a change in a of a factor of two, $\Delta\theta$ changes only in the third decimal place. Here the value of f_D is, of course, a linear function of angular spread (spot size).

Upon calculation, the value of f_D becomes

$$\Delta f_D = \frac{v_n}{\lambda_T}\left(\frac{(1.881)(2.54)}{\sqrt{(40)^2 + (1.881)(2.54)^2}} - \frac{(1.881)(2.54) - 0.02766}{\sqrt{(40)^2 + (1.881)(2.54) - .02766^2}}\right)$$

$$\Delta f_D = 6.8 \text{ kHz}. \qquad (42)$$

The values of the different frequency spreads increased as the Doppler frequency shift increased. The total experimentally determined frequency spread was 125 kHz at half peak height and 250 kHz at five percent of peak height under the conditions for the system discussed above.

G. Isofrequency Lines. Consider the scattering surface in the direction of propagation of the incident radiation. The Doppler frequency shift along the vertical axis was zero. The frequency along the horizontal axis increased linearly with distance (for small distances) on either side of the incident beam. When a hemisphere is constructed about the scattering center with its center at the scattering center and the perimeter of this hemisphere is transverse, the Doppler frequency increases from zero on the vertical axis to a maximum on either side at the horizontal axis then decreases to zero again at the negative vertical axis.

If a plane is cut through this hemisphere parallel to its flat surface and perpendicular to the incident beam and the Doppler frequency is plotted on this plane as a function of the spatial position, a family of isofrequency lines is generated which are hyperbolae with their vertices on the optical axis. The vertical axis is coincident with the conjugate axis of the hyperbolae and the horizontal axis is coincident with their tranverse axis. That is, the foci are on the horizontal axis and on either side of the

primary optical axis, and in the plane of the velocity vector, $\vec{v}$.

The eccentricity of each of these hyperbolae is large and approaches infinity near the vertical axis. In fact, the hyperbolae so nearly approximate a straight line that the negative distortion of the lens causes the curvature to change directions. The resultant experimental determination of the isofrequency lines contains the effects of the lens as well. The net curvature of the hyperbolae is small enough that within the limits of the lens edge a rectangular slit of the same width as the diameter of the limiting apertures can be used in their stead without significant increase in the Doppler frequency spread seen on the spectrum analyzer (see Figure 5 and Table 8).

H. Frequency Measurement Limits. There were several elements that could limit readout of the frequency information. Three spectrum analyzers were available for use in different regions of the frequency spectrum. For the rotating disc and laminar fluid flow this type readout was entirely suitable. For turbulent flow other techniques have been considered. One of the available spectrum analyzers (Tektronix 1L20) had an upper frequency limit of 4.2 GHz. This corresponds to a velocity of 2.54×10^6 cm/sec which was well beyond measured velocities. It was of the order of Mach 73. A tabulation of limiting factors is shown in Table 9.

The upper frequency limit of the photomultiplier tube with a 50 ohm anode resistor (used to match input impedance of Tektronix spectrum analyzers and C-Cor wide band amplifier) and a

liberally estimated 50 pF capacitance was 400 MHz. Assuming a linear Doppler shift, this gave a maximum of 242,000 cm/sec or Mach 7.3 which was not an unreasonably high velocity. Of course, associated circuitry, wiring, and electron transit time spread have an effect here, but generally the anode resistor R is the only really controllable factor.

Solid state detectors are available that have an upper frequency limit of 1.0 GHz but none of those commercially available have gain. (Types which do have gain are now in the development stage. Hewlett-Packard's pin photodiodes are as high as 1.0 GHz and have a quantum efficiency of 0.75 and dark current of 100 pA.). Therefore, it would be necessary to have high gain, wide-band amplifiers or a series of high-gain high-frequency slot amplifiers to use this upper frequency limit. Of course, a portion of this could be accomplished by using the amplifiers in the high frequency spectrum analyzer and the difference frequency generated in the spectrum analyzer circuitry. This frequency is low enough that the spectrum analyzer amplifiers can amplify it.

High frequency traveling wave tubes have recently been developed. They are, however, expensive and their long term characteristics have not yet been evaluated.

Another limit was the wideband Model 4366E C-Cor amplifier. It was perfectly matched to the photomultiplier and spectrum analyzer but its frequency response was 3 db down slightly above 200 MHz ($\pm$0.5 db down at 100 kHz and 155 MHz). If a linear

Doppler function were assumed, the maximum velocity would become 141,000 cm/sec or Mach 3.65, which is an appreciable velocity and above the generating capabilities of the equipment used in this study. The lower frequency limit of the C-Cor amplifier is 10 kHz, which permits 60 db amplification of any signal from 6 cm/sec to 141,000 cm/sec.

I. Noise. Noise, which was one of the major problems associated with the studies undertaken here, fell into two categories:

1. That noise which was inherent in the laser or was introduced into the optical circuit prior to the transformation of the optical signal to an electron current.
2. That noise that was developed in the photodetector or in subsequent amplifying and detection equipment. Since the electronic noise proved to be the lesser of the sources, it will be discussed first.

Since most of the noise was essentially white, any optical or electronic filter which attenuated it also would attenuate most of the desired signal. Table 10 presents a list of the noise sources.

1. Electronic Noise. With a photomultiplier in total darkness, a certain small amount of noise is detected at the output. The quantity of this noise is a function of the temperature within the photomultiplier. This is true because the source of the noise is random emission of thermal electrons which are then multiplied as they traverse the dynodes of the multiplier. This noise is called dark current and is a form of shot noise. It can be made

negligible for most work by refrigeration of the photomultiplier, although this method was not used for several reasons: the problems associated with securing and utilizing the refrigerant; the safety problems associated with personnel working around the refrigerant under conditions of no ambient lighting; and the measured values of dark current are so much lower than other sources of noise that it can be ignored. This was particularily true when using a spectrum analyzer readout, since this shot noise was spread out over a fairly broad frequency spectrum. Table 3 lists dark current values for the photomultipliers that were used on this research and measured at approximately 25° C. The high voltage power supply (Fluke Model 405B) for the photomultiplier was highly regulated, had high thermal stability, and had good long-term drift characteristics. The voltage divider was made of low-noise zener diodes bypassed by small capacitors to permit stable operation at both high and low frequencies.

b. Amplifier. The high-gain wideband C-Cor amplifier had an equivalent noise input of 40μ V and a 50 ohm input and output impedance. The 40μ V equivalent noise input was spread over a frequency range up to 200 MHz (i.e. the noise is 0.2μ V/MHz). In terms of the maximum IF bandwidth of a spectrum analyzer equal to 20 kHz, the noise became 0.01μ V. Here the noise was again insignificant. These figures were supplied by C-Cor.

c. Spectrum Analyzer. When an IF bandwidth of 5.0 kHz is assumed for a spectrum analyzer, the equivalent input noise

(Johnson or white noise) can be calculated from

$$N = \sqrt{4kT \Delta f R} \qquad (43)$$

where N = equivalent noise in volts

k = Boltzmann's constant = 1.38×10^{-23} joules deg^{-1}

T = temperature of the input resistor in degrees Kelvin (approximately 300° K)

Δf = frequency range of the signal or IF bandpass of the instrument

R = value of input resistance in ohms.

Table 20 contains the noise values for the spectrum analyzers that were used.

It should be noted that the noise figures quoted in Table 20 are worst case values. As the IF bandwidth is narrowed, the noise decreases as the square root of the bandwidth. In no case was this white noise the limiting factor, even though it could be seen on the 1L10 and 1L20 spectrum analyzers.

d. Stray Electrical Pickup. Most extraneous pickup was eliminated by the use of shielded cables necessary at high frequencies. Under certain conditions there was some R.F. feedthrough from the laser R.F. supply, but since it was a narrow frequency, it usually did not affect the readout. However, it prevented observation of data on an oscilloscope because of its large amplitude in the time domain.

2. Optical Noise.

a. Laser. The largest single source of noise was the laser. It consisted basically of three types:mode noise, plasma noise and spontaneous-emission noise.

The mode-interaction noise in the 50 mW Spectra-Physics Model 125 laser that was used was well defined, relatively stable and near zero frequency. Therefore, it did not introduce problems in readout on spectrum analyzers. However, it prevented the use of an oscilloscope readout.

The plasma and spontaneous-emission noise were continuously present. In the 0.8 mW Spectra-Physics Model 130B laser used in initial studies the best signal-to-noise ratio obtained was 4-to-1. In this case, the spontaneous noise was expected to be high. However, in the RF stabilized 50 mW laser the radio frequency waveform as well as strategically located ceramic magnets along the plasma tube were supposed to reduce this noise significantly according to Spectra-Physics who designed the tube. It was not possible to significantly reduce this noise. With about 100 times the power (the actual output of the Spectra-Physics 125 laser was 74 mW) of the small laser, the maximum signal-to-noise ratio was 13-to-1 using the DuMont 6911 and Amperex 150CVP photomultipliers.

b. Extraneous Coherent Light. All the components in the system scattered varying amounts of laser light. The output reflector of the laser cavity scattered appreciably. Since the laser beam traveled a rather large distance before it reached the rotating disc, much of the light scattered by the laser reflector was eliminated by placing apertures along the path of the incident radiation. However, there was some forward scattered light that transversed the apertures along with the incident beam.

Scattering also occurred from all reflectors, the surface-surface interfaces of the compound lenses, and the interfaces of the beam splitter and of the optical path length equalizer. The net result was to give a D.C. optical bias which contributed nothing to the signal but caused a higher background noise. This effectively lowered the modulation index of the heterodyned signal. Some of this noise was removed by limiting the portion of the photomultiplier cathode geometrically available to scattered rays.

c. Incoherent Light. Ambient light also contributed to the D.C. optical bias at the cathode of the photomultiplier. This light came from the plasma discharge of the laser, the hot cathode of the laser, fluorescence of cathode ray tube screens, scale light on cathode ray tubes, pilot light on auxillary measuring equipment, and room light.

The most important source of this noise (room light was eliminated by the unsatisfactory expedient of working without lights, posing a safety hazard. Pilot lights were removed and the hot cathode of the laser was covered, eliminating another important source of incoherent light. Because of overheating, the laser could not be covered for the long periods of time during which experiments were in process, leaving the plasma light as the major source of incoherence light noise. The light from the cathode ray tubes and scales were minimized, but of necessity remained on. Vacuum tubes were covered.

Other techniques were also used to help eliminate this incoherent light. Of course, the small photocathode area available to the coherent light helped to minimize noise of this type as well. In addition, an optical filter (low frequency band pass) attenuated any light with $\lambda<6000$ Å.

All of this difficulty with incoherent wideband light stemmed from a property of the photomultiplier with respect to light of wavelength 6328 Å. The photomultiplier was less sensitive to the 6328 Å line than to any shorter wavelength down to approximately 4500 Å. Since all the photomultipliers were more sensitive to a large range of wavelengths than they were to the narrow line at 6328 Å, low intensity sources emitting throughout this range of sensitivity created a large amplitude noise signal that was detrimental to the signal-to-noise ratio. That is, without limiting the wavelength of radiation entering the photomultipliers using small limiting apertures and optical filters, the white light to which the photomultiplier tube was sensitive would overshadow the narrow band of desirable red light.

d. Misalignment or Non-coincidence of Heterodyned Beams. If the beams to be heterodyned were not of the same size or were aligned such that they were not coaxial and did not form coterminous discs of light on the photomultiplier, an effective optical D.C. bias was again introduced. This occurred any time that light was present that was not being heterodyned with other light. It was not difficult to get a factor

of two increase in signal-to-noise by extra careful alignment as opposed to normal alignment of the beams. It can be seen that the size of the limiting apertures was critical in minimizing noise.

e. Unbalance in Heterodyned Beams Intensity. When the intensities of the two beams were not the same when they impinged on the photocathode, the modulation index deviated from unity and the noise increased. This was easily seen by beating the unattenuated light from the back of a laser with one of the scattered beams. In this case, only extremely careful alignment could pull the signal out of the noise.

f. Fine Lobe Structure of the Scattered Radiation. As predicted by Mie scattering theory, the large scattered lobes are made up of many finer lobes. If the two cylindrical beams defined by the limiting apertures are cut with a hypothetical plane perpendicular to their axes and the scattering surface is stationary, the two cylindrical beams produce two 3/16 inch diameter discs at the plane of intersection. The internal makeup of these two discs is a complex (and visually uncoordinated) series of light and dark splotches corresponding to the small scattered lobes and valleys respectively. The internal patterns of the two discs are generally completely different. When the two discs are superimposed such that their perimeters are coincident, there are significant areas of dark in disc #1 that fall on either dark or bright areas of disc #2 and vice versa. Of course, the superimposed dark areas produce no signal or noise. At the other extreme, the bright areas superimposed on dark areas produce all noise and no signal. If

areas from each of the two discs have different intensities, the modualtion index and noise generated is comensurate with their intensity ratio. Statistically there are areas on the two discs that are of equal intensity and, upon superimposing, the discs produce a modulation index of unity. It can be seen that the heterodyne efficiency of the system is low and that there is a large amount of noise introduced as a result.

The actual efficiency depends on the fine lobe structure developed at the scattering surface. As the scatterer moves, other discs appear with completely different internal structures leading to an infinite number of heterodyne combinations that are impossible to treat analytically.

Attempts were made to distribute the intensity of the lobes evenly throughout the area of the discs defined by the limiting apertures. Care was taken in this process to preserve the frequency profile of the two beams to enable cancellation of the frequency spread. The most obvious technique for doing this was to focus the two beams together onto the photocathode of the photomultiplier. The resultant heterodyne current was less than the current obtained with unfocused beams. Another technique that should have worked in theory was to rescatter the two beams using small scattering particles located close to the photocathode. This method also did not work well enough to be practical.

J. Intensity and Signal-to-Noise Ratio. The lack of intensity, or more accurately a low signal-to-noise ratio, was a difficult

problem to solve. The noise problem and its causes were discussed in the previous section. In this section some of the factors which limit intensity will be discussed. Signal-to-noise ratio is defined here as the ratio of the signal height from the baseline to the noise height from the baseline.

The fundamental limit on signal-to-noise was obviously the output of the laser itself. Since the noise in the laser radiation was optical, the signal-to-noise ratio was constant except for secondary phenomena which introduced non-linear effects. The Perkin Elmer Model 5200 laser used in initial studies had an output of 0.5 mW. Later a Spectra-Physics 130B laser with an output of 0.8 mW was used. For some critical determinations it was possible to use a 10 mW Spectra-Physics Model 112 laser. The use of the 10 mW laser facilitated certain studies because of the higher signal-to-noise ratio. Since the 10 mW laser was mounted on a one ton granite table, this also helped minimize vibration problems.

The use of a Spectra Physics 125 laser with an output of 72 mW at 6328 Å permitted a gain in signal-to-noise of a maximum of 13-to-1. By mounting the optical system on a granite table, signal fluctuations caused by room vibrations were minimized. Application of rf power to the laser increased laser output by 35.4 percent but did not significantly alter the noise level. All of the lasers used were diffraction limited and had plane polarized outputs.

Each of the system components contributed to the decrease in intensity. These components were picked to maximize intensity. Of course, the largest loss of intensity occurred at the scattering medium where an incident beam of about 40 mW of power was transformed into numerous scattered lobes with power in the nanowatt range. Except for the absorption loss in the scatterers, the sum of the powers of the lobes would be equal to the input power. Assuming that the scattered intensity was evenly distributed throughout the back hemisphere, each limiting aperture intercepted approximately 4 microwatts of power. Therefore, there was an automatic attenuation of 10,000 in intensity from the incident beam, making it imperative that the following and preceding components have maximum transmission efficiency. All power levels greater than 0.1 mW were measured by a Spectra-Physics Model 401 power meter.

1. Component Reflectivity. The commercially available mirrors and reflecting prisms used in the early studies lost between 11 and 32 percent by absorption. The gold mirrors which were made by vacuum evaporation absorbed less than 5 percent of light incident on them. The use of these gold mirrors permitted an increase in overall intensity impinging on the scatterers and permitted a closer balance of beam intensities in the heterodyne system. This produced a rise in heterodyne efficiency.

2. Lens. The original lens used in the optical network for

early experiments had a focal length of 8 inches and a diameter of 5 inches. These dimensions were ideally suited for the studies. However, the loss of light being transmitted through the lens was rather high because of the deterioration of the anti-reflective coatings and inhomogeneities in the lens. A corrected lens from a Tropel 4 inch collimator with a focal length of 40 cm and a 10 cm diameter with high quality anti-reflective coatings was used in later studies (see Figure 4). It had a transmission of 92.9 percent.

3. Beam Splitter. The beam splitter was the chief cause of signal attenuation in the optical heterodyne portion of the system. The original beam splitter used in the system had the following characteristics; absorption 54 percent; reflection 28 percent; and transmission 18 percent. The modulation index was 0.644. This beam splitter was an optical flat with one side coated with a reflecting dielectric which split the beam into two components.

These values can be used to discuss some problems involved in the beam splitter. Consider for a moment that all other aspects of the two beams impinging on the beam splitter are ideal: i.e. they are of uniform intensity, of equal intensity, and of the same size. More than half of each beam is immediately lost by absorption. Therefore, the heterodyne current is cut by a factor of two. In addition, only 18 percent of beam #1 beats with 28 percent of beam #2. Therefore, there is a large D.C. optical bias introduced which decreases the heterodyne current even more and introduces a large amount of noise.

In addition, 18 percent of beam #2 and 28 percent of beam #1 is thrown away because it exits from the beam splitter perpendicular to the beam which enters the photomultiplier. Attempts were made to use this beam as well (effectively doubling the signal) but with only partial success with this beam splitter. At times the heterodyne current was doubled; at other times it was cancelled. This was caused by a phase shift occurring at the beam splitter.

Replacement of the above beam splitter with a commercially available cube beam splitter eliminated the phase shift permitting an increase in the heterodyne current. This beam splitter had the following properties;absorption 8.9 percent, reflection 41.1 percent, and transmission 50 percent for one beam; and absorption 21.7 percent, reflection 28.3 percent, and transmission 50 percent for the other beam. The modulation indices were 0.822 and 0.566 respectively for ideal input beams. This led to a significant gain in heterodyne efficiency. However, there was still a large amount of coherent light that did nothing but contribute to the noise level. Of course, the ideal beam splitter would have 50-50 transmission-reflection for both beams. It was not too difficult to match transmittance-reflectance for one beam, but the absorption became large and the match did not hold for the other beam.

4. Longitudinal Mode Effects. The Spectra-Physics Model 125 laser operates in many longitudinal modes, which change the interference efficiency of two beams that are permitted to

interfere (in this case called heterodyning). A plot of heterodyne efficiency versus the number of laser cavity lengths nL between the two beams gives a curve such as that in Figure 13 (1). If the two beams have exactly the same length the interference is a maximum. This decreases rapidly as the difference in path lengths Δ increases. At $\Delta = 2L$ the interference is again a maximum as it will be at every interval of 2nL where n is an integer and L is the cavity length of the laser (148 cm). In the system used in this study, the value of Δ was such that the interference efficiency decreased about 40 percent. Two methods for correcting for this difference are readily obvious. First, Δ can be made to equal zero by folding the shorter beam with two mirrors to increase its path length to correspond to the other beam path length. This introduces two extra mirrors, each of which decreases the beam intensity by 5 percent. Two mirrors are necessary to fold the rays back to their original orientation to eliminate aperture size dependent frequency spread. This is not a good approach. Another technique was to introduce a material of high refractive index to make the shorter beam have an effective longer path length. To do this, the introduced medium must have a high refractive index to be reasonably short. This introduces several light losses at the glass-air interfaces. If the refractive index is kept at a reasonably small value to minimize interface losses, the medium must be rather long. Glass rods with plane-parallel faces are expensive. The length needed for material of n = 1.5 is about

7 cm. The technique that was used was to join two small right angle prisms on either side of a large right angle prism with Canada balsam to give a 7 cm retarding medium.

5. Beam Spread Effects. Since one of the scattered beams was more divergent than the other (which occurred because the lens was not corrected for light transversing it antiparallel to the incident radiation and since the beams were of different lengths), the signal-to-noise ratio was decreased. This problem was corrected by the procedures outlined for correcting path length difference.

6. Optical Filters. An optical filter placed in front of the laser helped attenuate some of the noise but it also contributed to a decrease in light available for scattering. Another filter placed immediately in front of the photomultiplier helped attenuate noise but also attenuated the desirable light input. The bandpass filters were Corning CS 2-63 with 78.6 percent transmission and Corning CS 2-61 with 83 percent transmission.

7. Spatial Filters. Spatial Filters were generally selected for efficiency. The spatial filters located throughout the optical network were greater than 99 percent efficient. The limiting apertures in the heterodyne system existed for the purpose of limiting transmission to the photomultiplier and the term efficiency does not apply. Their area was of course directly related to heterodyne current within limits of spatial coherence.

8. Photomultiplier. The particular line in the optical spectrum at which the He-Ne laser operates is undesirable in relation to

photomultiplier sensitivity. Any photocathode is at low values on its response curve at 6328 Å. Photocathodes that operate in this range have inherently low quantum efficiency; therefore, their response is low initially. The values for the photomultipliers used in this research are given in Table 12. An emitter follower was used between the photomultiplier and spectrum analyzer in early studies at low frequencies to permit matching the maximum possible load to the low input impedance of the spectrum analyzer. Each of the photomultipliers was more efficient and had higher sensitivity at shorter wavelengths (except for the S-1 response which was maximum at 8000 Å).

Quantum efficiency, radiant sensitivity and peak response were in general mutually exclusive. The RCA C70038D had the highest quantum efficiency and operated higher on the spectral response curve at 6328 Å but its radiant sensitivity was low. The RCA C70038D had a smaller photocathode area (0.65 x 0.5 inch) causing it to have little transit time spread. Therefore, it was used for high frequency work. A special voltage divider was constructed which permitted a flat frequency response from D.C. to over 400 MHz (depending upon the value of load). This divider was made with high tolerence zener diodes (1N4758A and 1N4759A) matched to give equal voltage drops at each stage and with each stage bypassed by a 1000 pF capacitor. Electrical leads were made short as possible. This configuration not only permitted high frequency response but also prevented loading of

later dynode stages. This divider with the RCA C70038D photomultiplier permitted signal-to-noise ratios as high as 80-to-1.

The other photomultiplier tubes had their own specialities with the 6911 being the tube employed in early low frequency studies. All of the photomultipliers were electrically shielded. This shield also served as an optical shield. In addition, the C70038D was double shielded. An inner shield of ferromagnetic metal was tied to the photocathode and acted as a magnetic--electric shield. A second concentric shield acted as an optical shield and an electrical insulator from the high voltage on the inner shield.

The intensity level was also increased by bringing both primary heterodyne beams in at less than 90° to the photocathode surface and multiply reflecting them back and forth onto the photocathode. This was possible because the photocathode had a high reflectance for nearly normal incidence.

9. Amplifier. A wideband C-Cor Model 4366E amplifier with 60 db gain was sometimes used between the photomultiplier and spectrum analyzer. It had an input and output resistance of 50 ohms and was matched to the 50 ohm load of the photomultiplier and 50 ohm input impedance of the spectrum analyzer to minimize signal loss at high frequency. Fifty ohm cables were used and kept as short as possible. This amplifier responded to rather rapid pulses (15 percent ringing for 1 nsec input step) because of its 3.0 nsec rise time.

K. Polarization Effects. Polarization played an important part in the determination of an optimized device. According to theory, the light scattered from dielectric Mie particles is always elliptically polarized; polarized light from conducting Mie particles always preserves the input polarization mode. Studies of the applicability of this theory to the existing system were made. It was necessary to determine if matching of $\vec{E}$ vectors of the two scattered beams would lead to an increased signal-to-noise ratio, what the characteristics of plane-polarized light scattered from metals would be, and to ascertain the extent of the redistribution of $\vec{E}$ vectors occurring with insulators.

A polarization rotator introduced in the unattenuated beam from the laser and rotated throughout its angular range showed that there was no measurable relationship between the polarization mode of the input beam and any of the characteristics of the scattered output beam. The absolute signal, absolute noise, signal-to-noise ratio, Doppler frequency, and frequency spread remained constant as predicted by Mie theory.

The polarization effects introduced by the gold reflecting mirrors are shown in Figure 6 and Table 13. This contribution was measured by putting the rotator in the laser beam after it was reflected by the gold mirror. The rotator was scanned throughout its angular range, and its transmitted power was measured on a power meter. The curve indicates a substantial amount of elliptical polarization occurring at the gold reflector. The same experimental

arrangement was used to determine the polarization effects introduced by the beam splitter. The results for both the reflected and transmitted beams are shown in Figure 7 and Table 14. The nonlinearity of these curves indicate how difficult it was to study other polarization effects by direct rotation of the $\vec{E}$ vector. The transmission of the polarization rotator was a constant 95.5 percent at all angles.

The polarization properties of the radiation backscattered from the Mie particles were studied with the idea of then matching $\vec{E}$ vectors of the two mixed beams to increase the signal-to-noise ratio. A polarizing material was placed in each leg of the heterodyne system immediately after the limiting apertures. The polarization rotator was placed in one leg immediately after the polarizer. The polarizers converted the light from the lens into plane-polarized light. The rotator in one leg was then adjusted until a maximum signal-to-noise ratio occurred. This happened when the $\vec{E}$ vectors of both legs were parallel to each other. One of the polarizers was then rotated through a known angle and the rotator adjusted until maximum signal-to-noise ratio again occurred. This happened when the $\vec{E}$ vectors of both legs were parallel to each other. One of the polarizers was then rotated through a known angle and the rotator adjusted until maximum signal-to-noise ratio again occurred. By going through a series of similar steps it was possible to determine what the maximum possible signal-to-noise ratio was. This value was approximately 70-to-1 compared to the lowest maximum of 55-to-1 and a signal--

to-noise ratio of 80-to-1 without polarizers or rotator. When the two $\vec{E}$ vectors were perpendicular, the signal-to-noise ratio was 4-to-1.

There were several effects which affected the readout. First the mirror and beam splitter in the mixing circuit contributed significantly to the change in signal. Secondly, approximately half of each beam was absorbed in the polarizers. Thirdly, there was an imbalance introduced by the presence of the rotator in one of the beams.

Another approach yielded more information on the elliptical polarization of the scattered beams. The study of the static lobes radiating from the scattering medium indicated that within the individual lobes elliptical polarization did exist. However, some of the lobes could be extinguished by means of a polarizer, indicating the presence of some plane-polarization. Of course, this is only a special form of elliptical polarization. The smaller the area of the sample, the greater the tendency there was for the lobe to appear as if it were completely plane-polarized. This was simply a readout problem. The eccentricity of the polarization ellipse as well as the direction of its axes changed with the change in size of sampling aperture. Contours of equivalent $\vec{E}$ vector orientations were seen by placing a rotator and a polarizer in a scattered beam and studying the resultant pattern on a screen. The contours were not discontinuous but were intensity modulated by the lobes and nulls of the scattering pattern.

The study of a moving medium yielded more complete and useful information. A long time constant voltmeter was used to read out the data in order to integrate the modulation introduced by constantly changing lobe patterns. The rotator and polarizer were placed in a scattered beam at an angle of 30° with respect to the incident beam. As the rotator was scanned, the effective length of the $\vec{E}$ vector in a given direction was ascertained. The aperture did not affect the directions of the axes of the polarization ellipse. The velocity of the moving medium also had no effect on the polarization properties of the scattered light. The effect of aperture diameter on the eccentricity of the polarization ellipse is given in Table 15. The lengthening of the major axis with a decrease in aperture size is in complete agreement with data obtained with the static lobes.

A similar measurement was made with the above equipment setup in each leg of the heterodyning system. It was placed before the mirror and beam splitter respectively. The resultant major-to-minor axis ratios were equal to each other at a value of 1.49.

A metal disc yielded higher signal-to-noise ratios than did the dielectric scatterers. This occurred because of the lobe backscattered adjacent to and around the incident radiation. The maximum signal-to-noise ratio was 143-to-1. The backscattered light was plane-polarized but the two heterodyned beams were of unequal intensity as indicated by a second harmonic of the Doppler

signal with a signal-to-noise ratio of 7.5-to-1 and a third harmonic of 1.5-to-1 signal to noise ratio.

The direction of the $\vec{E}$ vector for maximum and minimum intensities was measured at several observation angles. The rotator and polarizer wereagain placed in the scattered radiation without benefit of the lens. The results of this study are given in Table 16. The ratios of the major-to-minor axes of the polarization ellipse were significantly greater for the metal scatterers than for the dielectric scatterers. This indicates that the radiation scattered from the metal is practically plane-polarized agreeing with Mie scattering theory.

L. Solid Volume Scatterers. The volume made of optical quality silicone resin with suspended particles from 3M Velvet Coating was studied to determine the effects caused by a three-dimensional scatterer upon the readout data. The concentration was chosen to make the scattering independent as determined by the particle separation being greater than three times the radius of the particles. Single scattering was guaranteed by making the concentration sufficiently low that doubling the concentration simply doubled the scattered light intensity. The motor was mounted such that its axis was perpendicular to the incident light beam. The velocity vector of the scatterers remained perpendicular to the incident beam and to the motor axis.

The silicone volume was moved along the path of the incident beam. This changed the position of the focal point within the

the volume. A plot of Doppler frequency obtained with a spectrum analyzer versus the depth of the focal point within the volume yielded a linear relationship. This would be anticipated since the relationship between particle velocity, the radius on which sampling occurs, and the Doppler frequency shift were earlier shown to be linearly related for small sampling angles. The linear relationship indicates that the sampling volume was not being shifted in relation to the focal point as the focus occurred deeper within the volume.

The intensity of the light scattered from the volume was a maximum when the incident light was focused on the surface of the silicone volume. As the focal point was positioned immediately in front of the surface, the intensity immediately decreased to zero. As the focal point was positioned immediately behind the surface within the silicone, the intensity began falling off, reaching a plateau rapidly. This intensity plateau was maintained until the focus occurred on a metal cylinder which was coaxially positioned about the motor shaft to help support the silicone volume. At this point a second maximum was reached which indicated the stronger scattering from the metal surface. The practically constant value of intensity from within the silicone indicated there was little change in sampling volume. The rather sharp decrease in intensity when scanning the focal point through the silicone-air interface indicated a short sampling volume.

The light intercepted by the limiting apertures was spread out over an elliptical area, indicating backscattered rays were coming from a finite volume rather than a point. By selecting

the portion of this ellipse which interfered, the sampling volume could be varied. This could be done in two ways. First the rays could be reflected through a long path so that the rays could diverge. A slit or aperture could intercept a portion of this expanded ellipse to select a small effective sampling volume in the silicone. Another technique would be to focus the mixed beams with an aplanatic lens. A pinhole could be placed at the focal point to select the small segment of rays corresponding to the small sample volume in the silicone.

M. Liquid Volume Scatterers. The flowing liquid system was studied to determine if any additional effects were contributed by a three-dimensional laminar flow as opposed to two- and three--dimensional solid scatterers. Care was taken to eliminate bubbles from the flowing stream. However, after air bubbles were inadvertantly introduced, it was found that their contribution to the backscattered intensity was negligible. This should have been anticipated because of the large difference in transmission of air bubbles and the 3M Nexel Velvet Coating particles suspended in the flowing stream.

The low velocity of the flowing liquid placed the Doppler frequency peak in the region of severe longitudinal mode noise on the spectrum analyzer display. This made it necessary to vary the velocity of the flowing stream to place the frequency peak between noise peaks. This severely limited the versatility of the system. The width of the frequency peak appeared to be determined by the 50 kHz spectrum analyzer line width rather than by characteristics of the flowing stream. The value of Doppler frequency was approxi-

mately 250 kHz which corresponds to a particle velocity of less than 10 cm/sec which is well within the laminar flow region for the configuration of flowing system used.

The particles which collected on the inside of the window used for viewing the flowing stream, caused surface scattering to be predominant. However, the lever arm technique for limiting scattering volume discussed in the section on solid volume scatterers was used to eliminate this scattering and to select the region of the scattering volume desired. The pinhole technique of volume selection was not tested for liquid volume scatterers, but it should be as satisfactory for this use as it was for solid volume scatterers.

The evolutionary process toward an optimized "velocimeter" involved the study of all the parameters that could contribute to a deterioration in the readout or to ambiguities in the readout. It also involved a study of the parameters that could contribute to a better readout and understanding of this readout. The final result of this study is given in outline form in Figure 14.

VII. CONCLUSIONS

It was possible to optimize the geometrical configuration of the laser Doppler "velocimeter". The optimum geometry demands a symmetrically heterodyned sampling system with heterodyning occurring between two scattered beams rather than between a beam that is frequency shifted and one which is not frequency shifted. This arrangement minimizes some sources of noise and eliminates frequency spread caused by a finite aperture size.

The laser contributes the major portion of noise in the readout spectrum. This noise is white and cannot be eliminated by filtering. The beam splitter in the heterodyne network contributes to a significant loss in signal because of beam imbalance and absorption. Light scattered from dielectric Mie particles is elliptically polarized; that from metal particles is linearly polarized. Fine lobe structure, inherent in scattering of coherent light from Mie particles, is the major cause of loss of heterodyne efficiency because of the low probability of complete overlap of the entire volume of the two heterodyned beams. Longitudinal moding of the laser, misalignment and lack of coincidence of the heterodyned beams, and the beam splitter are the other major causes of loss of heterodyne efficiency.

Inherent frequency spread for a given IF bandwidth, sweep width, and sweep rate in the spectrum analyzer are major causes of Doppler frequency spread on the display CRT of the spectrum analyzer.

The vertical dimension of the focused input beam intercepts a finite spread of velocities and therefore causes a frequency spread. The horizontal dimension of the focused input beam is analogous to an uncertainty in observation angle and as such also represents a frequency spread.

The effects of particle size, particle size distribution, and particle shape can be neglected only if the criteria for Mie's original theory of spherical particles are met. These criteria are easily met. The existence of practically linear isofrequency contours in the backscattered radiation permit use of rectangular apertures rather than the small circular apertures. This is true within the angular limits determined by the lens aperture.

BIBLIOGRAPHY

1. Ballard, G. S., Private communication.

2. Brown, E.B., "Modern Optics", Rheinhold Publishing Corp., London, (1965).

3. Carlin, P.W., Proc. IEEE, 52; 1371 (1964).

4. Condon, E.U. and Odishaw, H., "Handbook of Physics", McGraw-Hill Book Co., New York (1958).

5. Dodd, J.G., Private communication.

6. Foreman, J.W., George, E.W., and Jetton, J.L.,"Gas Velocity Measurement Using Scattering Techniques", Tech. Note R-178,Jan 1966.

7. Goldstein, R.J. and Kreid, D.K., Trans. of the ASME J. of Applied Mechanics, 34; 813 (1967).

8. Gould, G., Jacobs, S.F., LaTourrette, J.T., Newstein, M. and Rabinowitz, P., Applied Optics, 3; 648 (1964).

9. Hass, G. and Ritter, E.J. of Vacuum Science and Technology, 4; 71 (1967).

10. Lee, C.Q., "An Investigation of Photoelectrically Heterodyning Coherent Light", Astrionics Research and Development No. 2.

11. Mie, G., Annalen der Physik, 24; 377 (1908).

12. Renau, J. and Collinson, J.A., The Bell System Technical J., 44; 2203 (1962).

13. Ridgen, J.D., and Gordon, E.I., Proc. IRE, 50; 2367 (1962).

14. Spectra-Physics Laser Technical Bulletin No. 5, p. 8.

15. van de Hulst, H.C., "Light Scattering by Small Particles", John Wiley and Sons,Inc., London (1957).

16. Wankum, D.L., Private communication.

17. Yea, Y. and Cummins, H.Z., Appl. Phys. Let., 4; 176 (1964).

TABLE 1

LASER CHARACTERISTICS

Laser	Rated Output Power	Relative Noise	Major Use
Spectra-Physics 112	10 mW	High	Study of Scatterers
Spectra-Physics 125	50 mW	Lowest	Other Studies
Spectra-Physics 130	1 mW	Highest	Study of Scatterers
Perkin Elmer PE 5200	0.5 mW	High	Study of Scatterers

TABLE 2

SPECTRUM ANALYZER CHARACTERISTICS

Spectrum	Resolution (IF Bandwidth) (kHz)	Dispersion (Sweepwidth) (kHz/cm)	Sweep Rate (sec/cm)
Singer SPA-3/25a	0.2-25	0.3-300	$0.1 \rightarrow 10^{-3}$
Tektronix 1L10	0.01-1	0.01-2	$<1 \rightarrow 5 \times 10^{-3}$
Tektronix 1L20	1-100	$1-10^{4}$	$<1 \rightarrow 5 \times 10^{-3}$

TABLE 3

PHOTOMULTIPLIER CHARACTERISTICS

Photomultiplier	Dark Current	Response	Equivalent Noise Output (R = 50 Ω)
DuMont 6911	15.0 μA	S1	0.75 mV
Amperex 150CVP	10.0 μA	S1	0.5 mV
RCA C70038D	1.3 nA	Special	0.065 μV

TABLE 4

SCATTERERS STUDIED

Material	Preparation	Type Centers	Scattering Pattern	Scattered Intensity
Aluminum	Sandblast	Uniform	Shaped	Poor
Aluminum	SiC	Uniform	Shaped	7/1
Steel	Al_2O_3	Flat	Shaped	Poor
Steel	SiC	Random	Shaped	7/1
Graphite	None	Platelets	Shaped	Very Poor
Carbon	Deposition	Random	Shaped	Very Poor
Paper	None	Cylindrical	Multilobed	Poor
Plexiglas	Sandblast	Uniform	Shaped	1.5/1
Plexiglas	Chemical	Non-Uniform	Variable	Variable
Glass Beads	None	Spheres	Uniform	Poor
Mycalex	None	Non-Uniform	Variable	Variable
Enamel	On Substrate	Uniform	Isotropic	4/1
Pigment	On Substrate	Uniform	Isotropic	4/1
Willemite	Deposition	Random	Isotropic	Good
Teflon	None	Unknown	Dependent	Good
Polyethylene	Polish	Globules	Dependent	Good

TABLE 5

MISALIGNMENT CAUSES OF INEFFICIENT HETERODYNING

Cause	Mathematical Factor
Angular separation between two parallel beams.	Exponential
Spatial separation between two parallel beams which are also mutually parallel.	Exponential
Misalignment of the major axes of the polarization ellipses of the scattered rays.	Cosine
Deviation of one or both of the heterodyning beams from parallel	Exponential

See Lee (10)

TABLE 6

RELATION OF f_D TO θ

Observation Angle (θ)	f_D Approx. (MHz)	f_D Exact (MHz)	% Error
17° 20'	27.7768	27.3554	1.54
15°	24.0380	23.7644	1.15
10°	16.0250	15.9442	0.51
6° 32'	10.4700	10.4470	0.22
6°	9.6152	9.5978	0.18
5° 31'	8.8402	8.8274	0.15
5°	8.0130	8.0028	0.13

TABLE 7

RESULTS OF FREQUENCY SPREAD STUDIES

Effect	Magnitude of Contribution
Size of Limiting Aperture	* No Contribution
Particle Size	* No Contribution
Particle Size Distribution	*No Contribution
Variations in Motor Velocity	*No Contribution
Movement Parallel to Optic Axis	*No Contribution
Beam Convergence	*No Contribution
Vertical Focal Diameter	12.4 kHz
Horizontal Focal Diameter	6.8 kHz
Spectrum Analyzer	50.0 kHz

*Under conditions discussed in the section on "Discussion of Results"

TABLE 8

EFFECT OF ISOFREQUENCY LINES

Distance above Optical Plane (Inches)	Doppler Frequency (MHz)
0.00	4.900
0.30	4.950
0.60	4.975
0.90	4.985

TABLE 9

FREQUENCY MEASUREMENT LIMITS

Limiting Component	Frequency Limits	Velocity Limits (cm/sec)	Velocity Limits (Mach Number)
Singer SPA-3/25a	200Hz-25MHz	$0.121\text{-}15.1\times10^{3}$	$3.65\times10^{-6}\text{-}0.42$
Tektronix 1L10	1MHz-36MHz	$605\text{-}21.8\times10^{3}$	0.0182-0.657
Tektronix 1L20	10MHz-4.2GHz	$6.05\times10^{3}\text{-}2.54\times10^{6}$	0.182-76.7
RCA C70038D	D.C.-400MHz	$0.0\text{-}0.254\times10^{6}$	0.0-7.3
C-Cor Amplifier	10kHz-200MHz	$6.0\text{-}0.141\times10^{6}$	$0.73\times10^{-6}\text{-}3.65$

TABLE 10

NOISE SOURCES

Noise Source	Significance of Noise	Magnitude
Photomultiplier	No significance	0.065 μV
Amplifier	No significance	0.01 μV
Singer SPA-3/25a	No significance	0.155 μV
1L10	No significance	0.0288 μV
1L20	No significance	0.288 μV
Stray pickup (laser)	Factor only at high frequency	-----
Stray pickup (other)	Factor only at low frequency	-----
Laser Mode Noise	Factor only at low frequency	≈0.1 mV
Laser plasma and other white noise	Throughout spectrum. Of major significance.	≈0.01 mV
Extraneous coherent light	Can be made minimal	-----
Incoherent light	Was practically eliminated	Below detection limit
Condition of heterodyned beams	Significant	Theoretical treatment

TABLE 11

SOURCES OF SIGNAL LOSS

Component	Cause of Decrease in Signal	Relative Contribution
Laser	Nonlinear S/N output	Primary
Reflectors	Absorption	Minor (5%)
Lens	Absorption, scattering	Minor (8.1%)
Scatterer	Isotropic scattering	Major (99.99%)
Beam splitter	Absorption, reflection, transmission	Major (Depends on beam)
Longitudinal modes	Coherence length of laser	Significant (Depends on ΔL)
Beam spread	Non-coaxial beams	Minor
Optical filters	Absorption	Significant (18-21.4%)
Spatial filters	Geometric shadowing	Minor (< 1.0%)
Photomultiplier	Loss of response Wide bandwidth	Significant (25-30%) Large (Unknown)
Amplifier	Loss of frequency response	3 db at 15 kHz and 200 MHz
Polarization	Misalignment of $\vec{E}$ vectors	Minor (cosine function)
Volumes	Surface effects	Significant

TABLE 12

PHOTOMULTIPLIER SIGNAL CHARACTERISTICS

Photo-multiplier	Percent Quantum Efficiency	Sensitivity (Radiant A/W)	Percent of Maximum Response	Wavelength of Maximum Response
DuMont 6911	0.36	1,750	70	8000
Amperex 150CVP	0.36	6,750	70	8000
RCA C70038D	25.00	3,750	75	5500

TABLE 13

EFFECTS OF GOLD MIRRORS ON POLARIZATION

Rotator Angle (Degrees)	Power Reflected (%)	Rotator Angle (Degrees)	Power Reflected (%)
10	80.6	122	87.1
22	82.2	132	85.5
30	83.9	140	83.9
38	85.5	150	82.2
50	87.1	162	80.6
64	88.7	170	80.6
84	90.4	180	80.6
116	88.7		

TABLE 14

EFFECTS OF BEAM SPLITTER ON POLARIZATION

Rotator Angle (Degrees)	Reflected Power (%)	Transmitted Power (%)
0	11.0	33.9
10	11.3	33.6
20	11.9	32.3
30	13.2	27.8
40	15.0	25.0
50	18.4	22.6
60	18.5	20.5
70	19.8	19.2
80	21.0	18.5
90	21.3	19.0
100	21.0	19.0
110	20.2	20.2
120	18.9	22.3
130	17.3	24.7
140	15.5	27.4
150	13.7	30.2
160	12.4	32.3
170	11.3	33.7
180	11.0	33.9

TABLE 15

THE EFFECTS OF SAMPLING AREA ON POLARIZATION

Aperture Diameter (inches)	Ratio of Major to Minor Axis
0.281	1.05
0.250	1.07
0.219	1.11
0.188	1.14
0.156	1.16
0.125	1.19
0.094	1.19

TABLE 16

RELATION OF SCATTERING ANGLE AND $\vec{E}$ VECTOR DIRECTION

Sampling Angle (θ)	$\vec{E}_{max}$	$\vec{E}_{min}$	Material	Major to Minor Axis
25	699.0	611.0	Dielectric	1.2/1
45	No variation here		Dielectric	1/1
70	583.0	674.0	Dielectric	1.1/1
45	50.5	681.0	Metal	27/1
65	50.0	680.5	Metal	27/1
70	50.0	680.5	Metal	27/1

TABLE 17

FREQUENCY DISTRIBUTION AT APERTURE PLATE

Aperture	Center	Top Edge	Bottom Edge
#1	$f + 2\delta f$	$f + 3\delta f$	$f + \delta f$
#2	$f - 2\delta f$	$f - \delta f$	$f - 3\delta f$
#3	f	f	f

TABLE 18

EFFECT OF CONVERGENCE ANGLE

Limit	θ	Ψ	f_D (MHz)
min	5° 50'	89° 50'	1.016
max	6° 10'	90° 10'	1.074

TABLE 19

CALCULATED EFFECT OF CONVERGENCE ANGLE

Limit	Θ	Ψ	f_D (MHz)
min	2° 30'	86° 30'	0.436
max	9° 30'	93° 30'	1.639

TABLE 20

NOISE AND INPUT IMPEDANCE OF SPECTRUM ANALYZERS

Spectrum Analyzer	Maximum IF Bandwidth, Δf	Input Impedance Z_i	Equivalent Noise
Singer	20 kHz	72 Ω	0.155 μV
1L10	1 kHz	50 Ω	0.0288 μV
1L20	100 kHz	50 Ω	0.288 μV

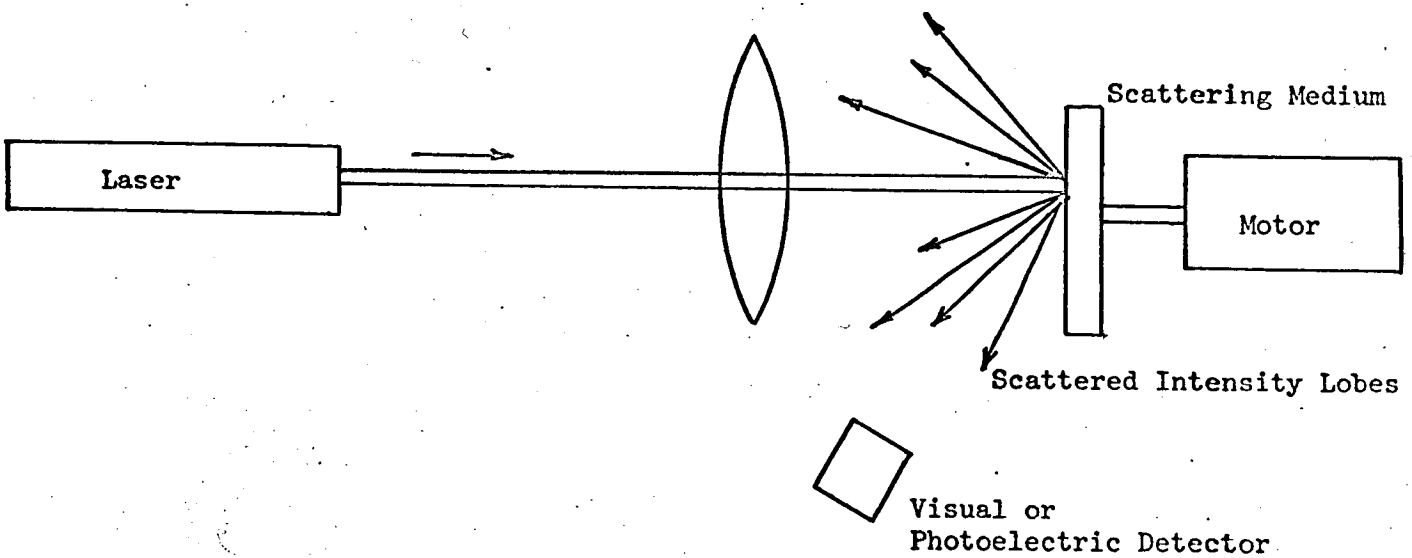

Figure 1

APPARATUS FOR DETERMINING THE SCATTERING CHARACTERISTICS OF SCATTERING MEDIA

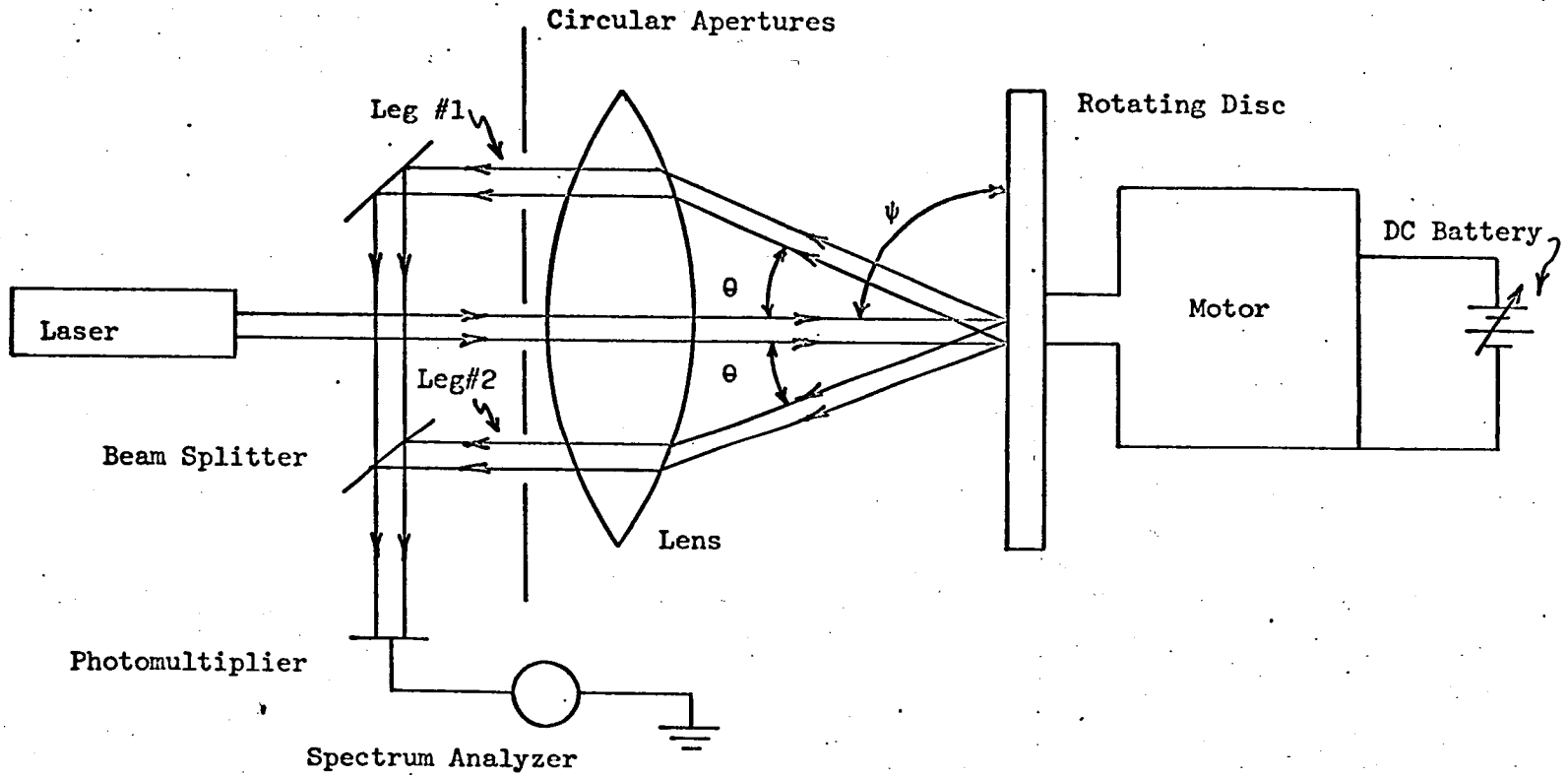

Figure 2

BASIC EXPERIMENTAL ARRANGEMENT FOR STUDYING SYSTEM PARAMETERS USING A SYMMETRIC HETERODYNE CONFIGURATION

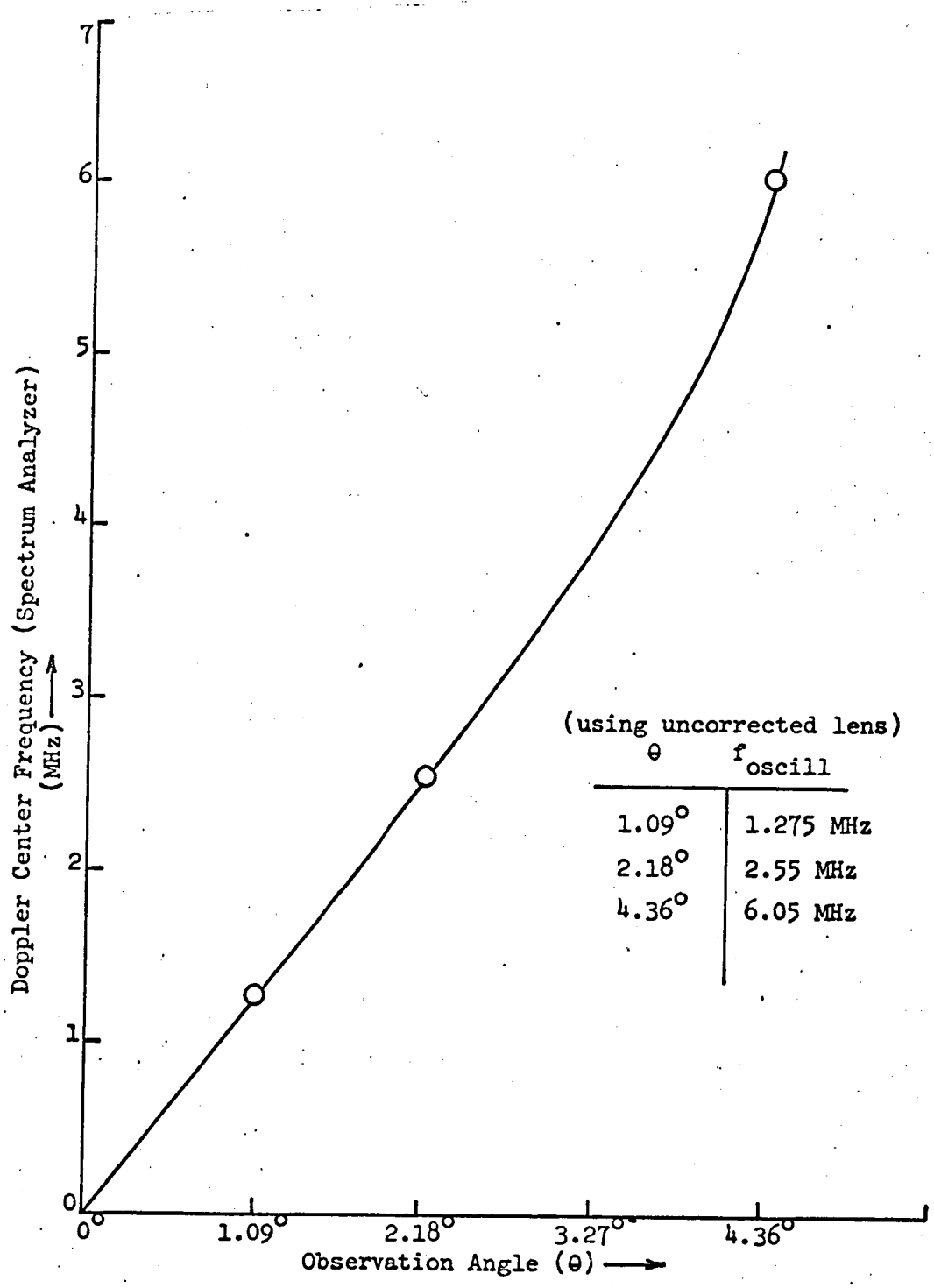

Figure 3

FREQUENCY READOUT ERROR CAUSED BY DISTORTIONS IN UNCORRECTED LENS

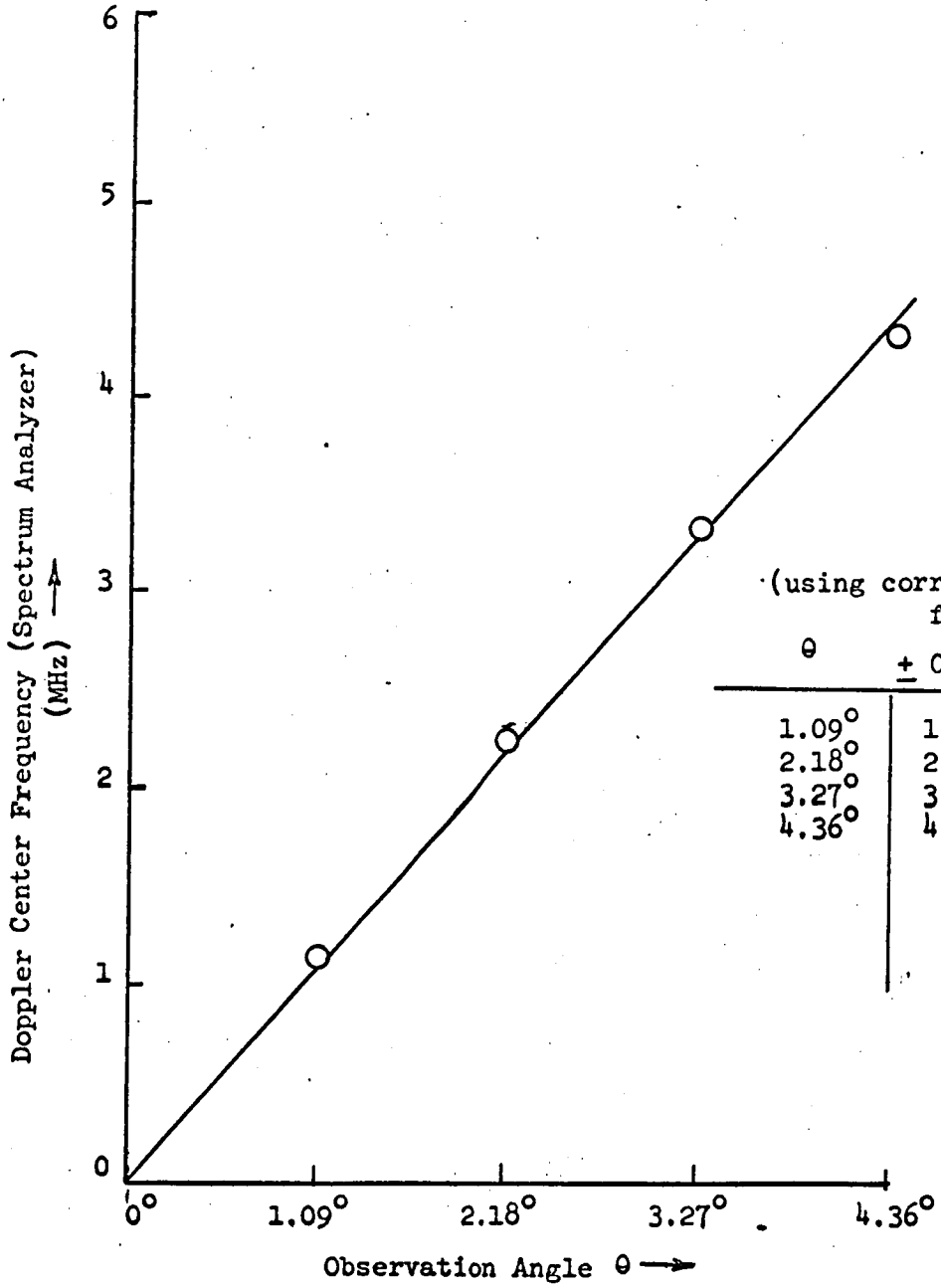

(using corrected lens)

θ	f_{oscill} ± 0.005 MHz
1.09°	1.150 MHz
2.18°	2.250 MHz
3.27°	3.350 MHz
4.36°	4.355 MHz

Figure 4

FREQUENCY READOUT ERROR FOR CORRECTED LENS

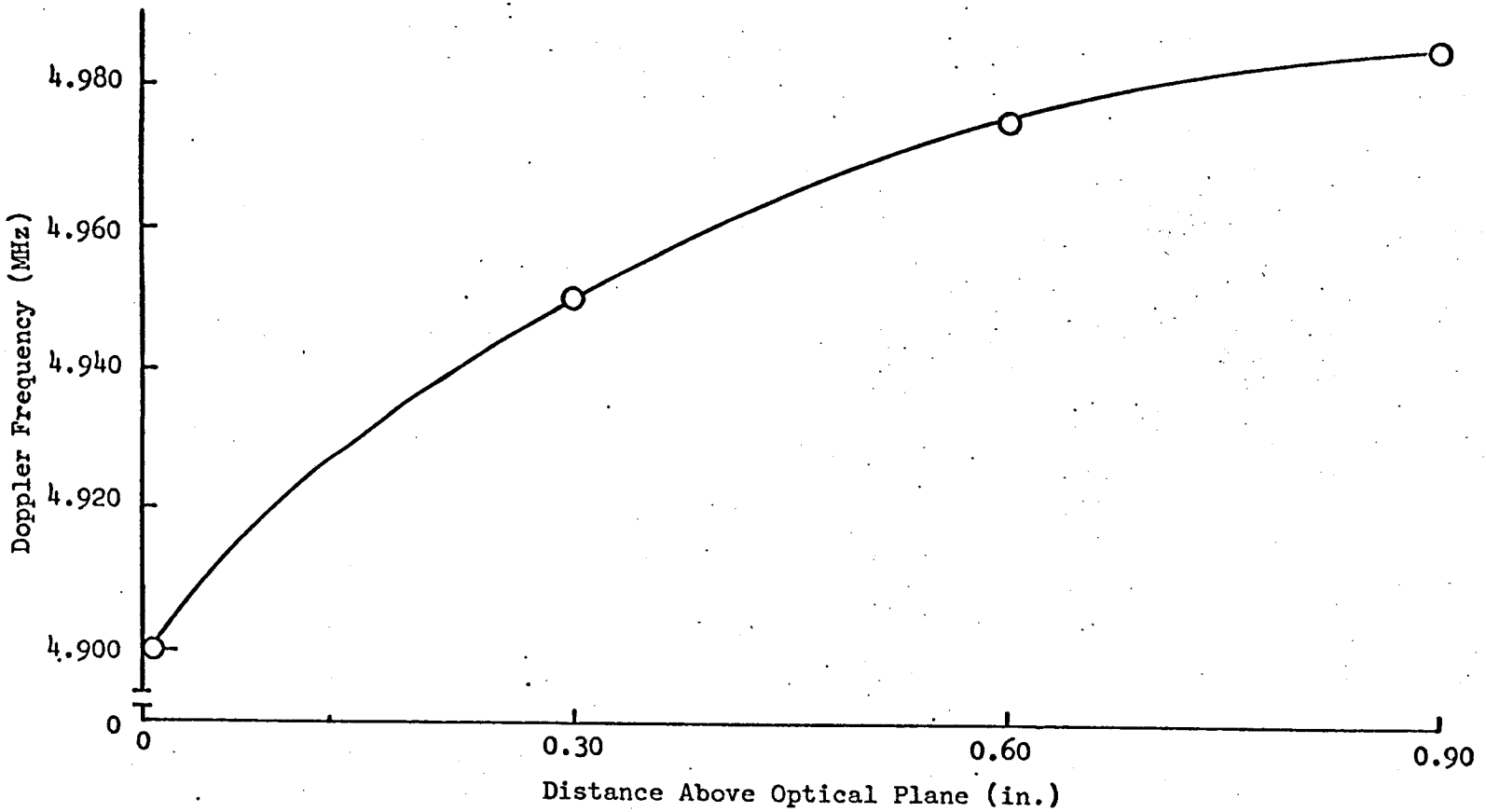

Figure 5

EFFECT OF CURVATURE OF ISOFREQUENCY LINES ON DOPPLER FREQUENCY MEASURED ON A LINE PERPENDICULAR TO THE OBSERVATION PLANE AND OFF THE OPTICAL AXIS

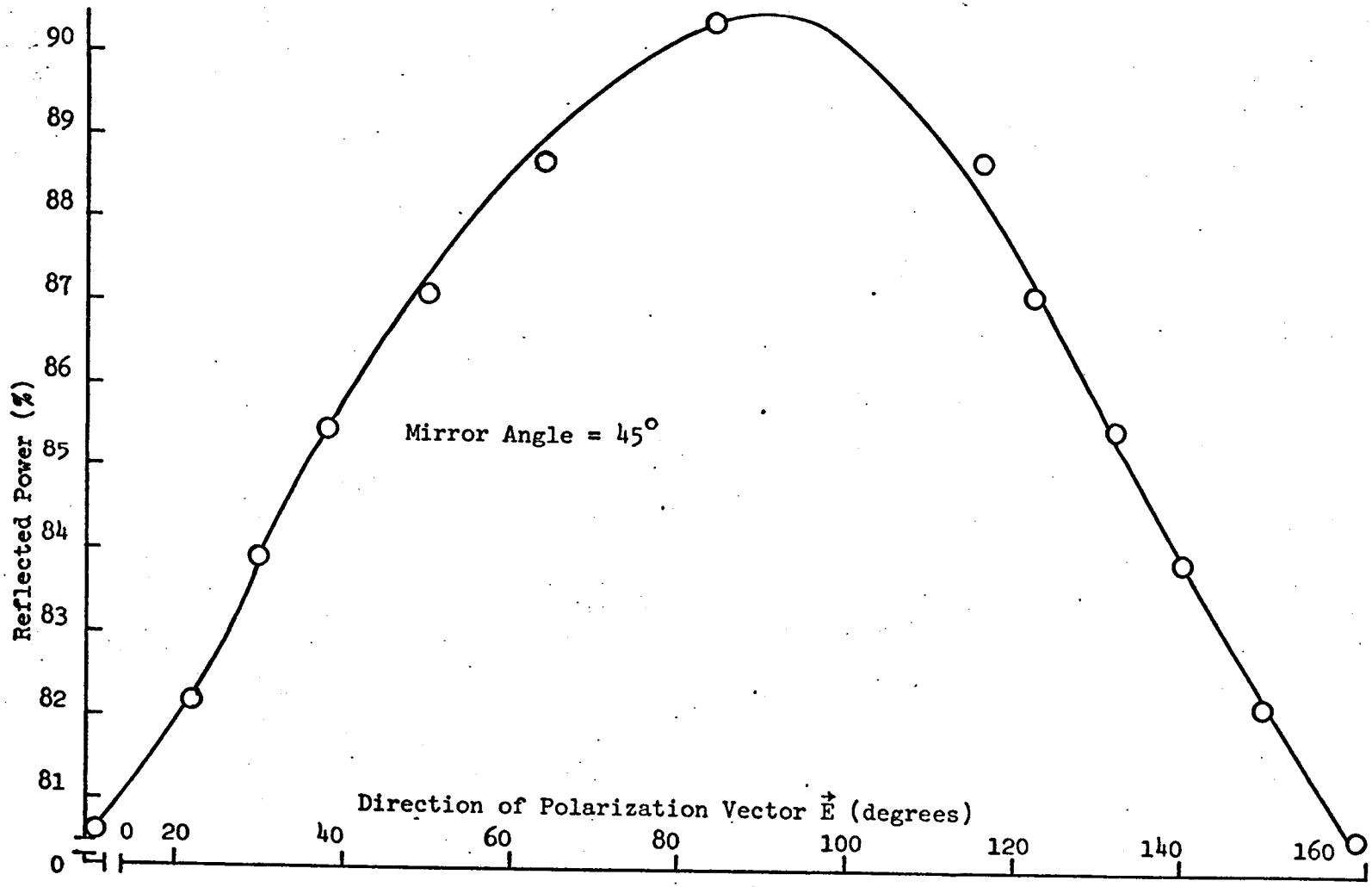

Figure 6

EFFECT OF GOLD MIRROR ON THE POLARIZATION VECTOR $\vec{E}$ AS IT IS ROTATED BY A POLARIZATION ROTATOR

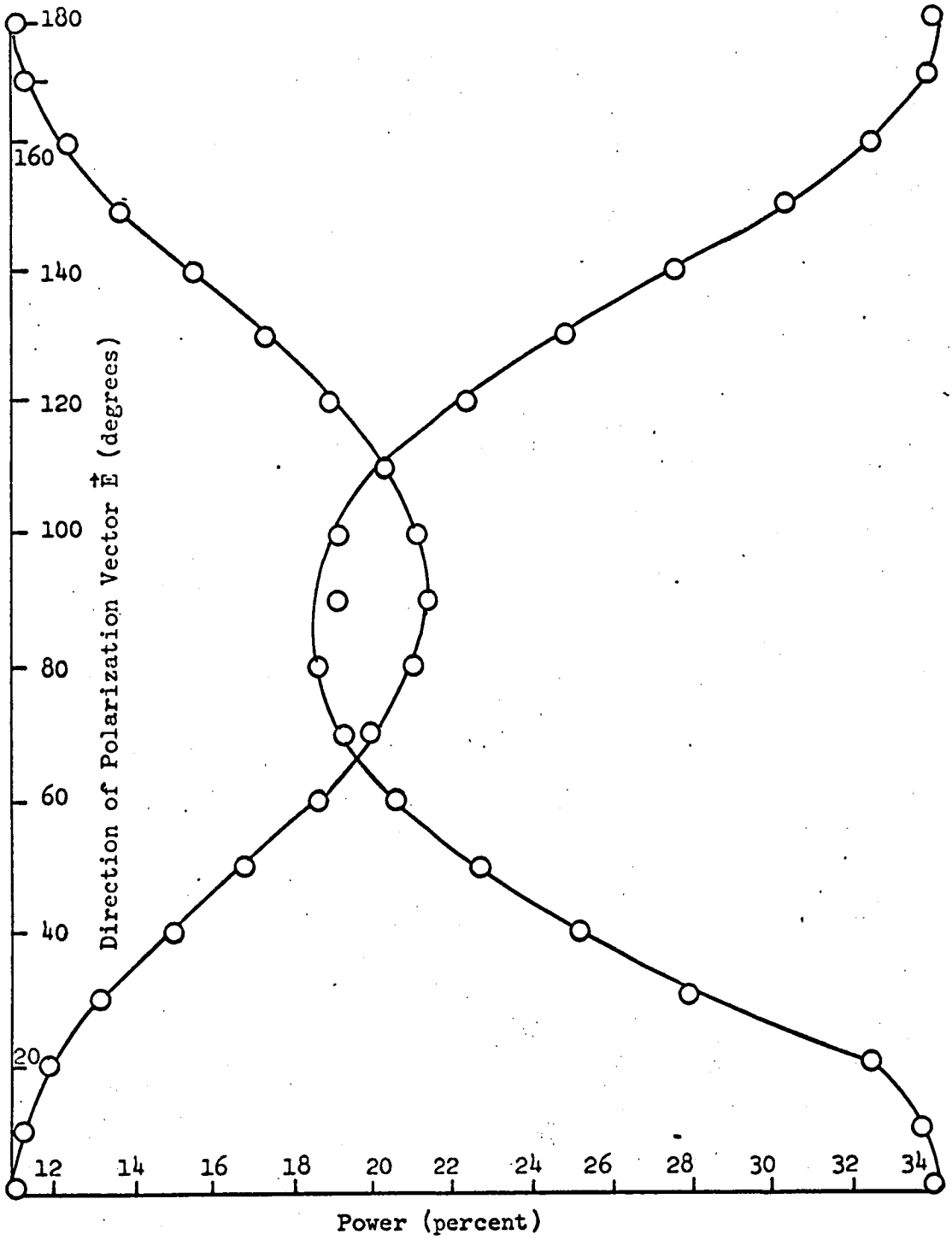

Figure 7

EFFECT OF BEAM SPLITTER ON POLARIZATION VECTOR $\vec{E}$

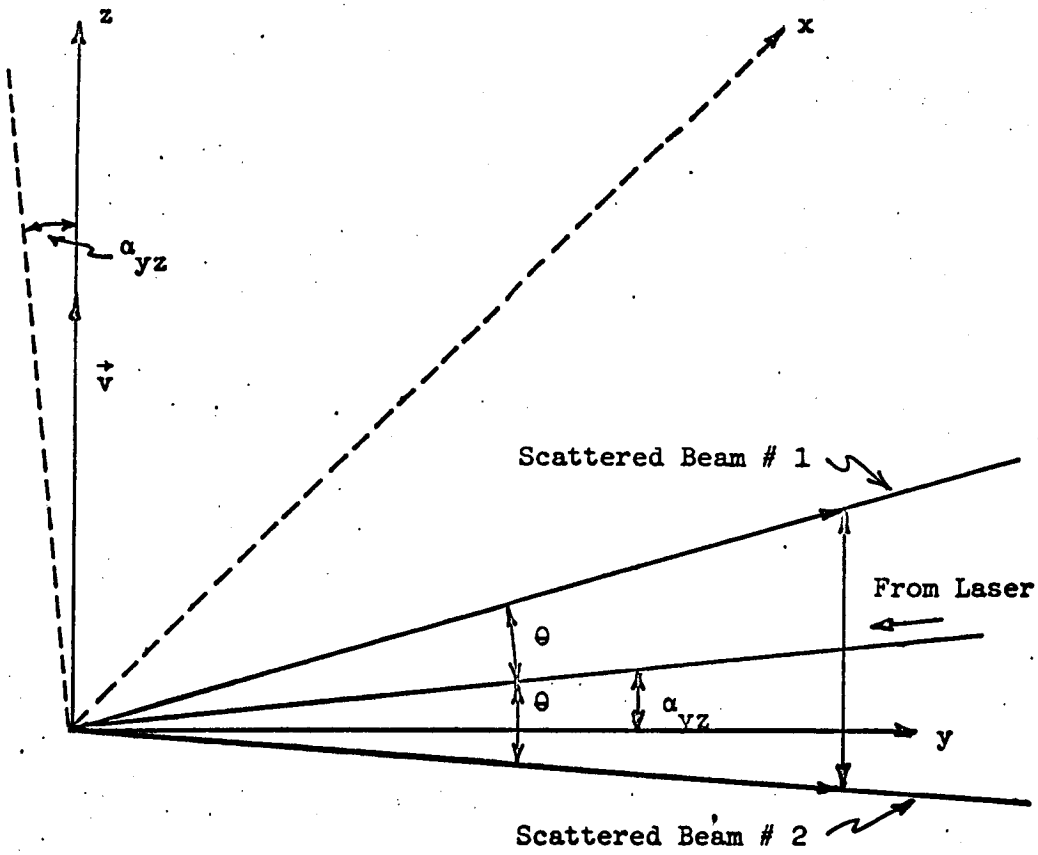

Figure 8

VECTOR-ANGLE DIAGRAM USED IN DERIVATION OF DOPPLER EQUATION WHEN THE INCIDENT LIGHT IS NOT NORMAL TO THE VELOCITY VECTOR, $\vec{v}$

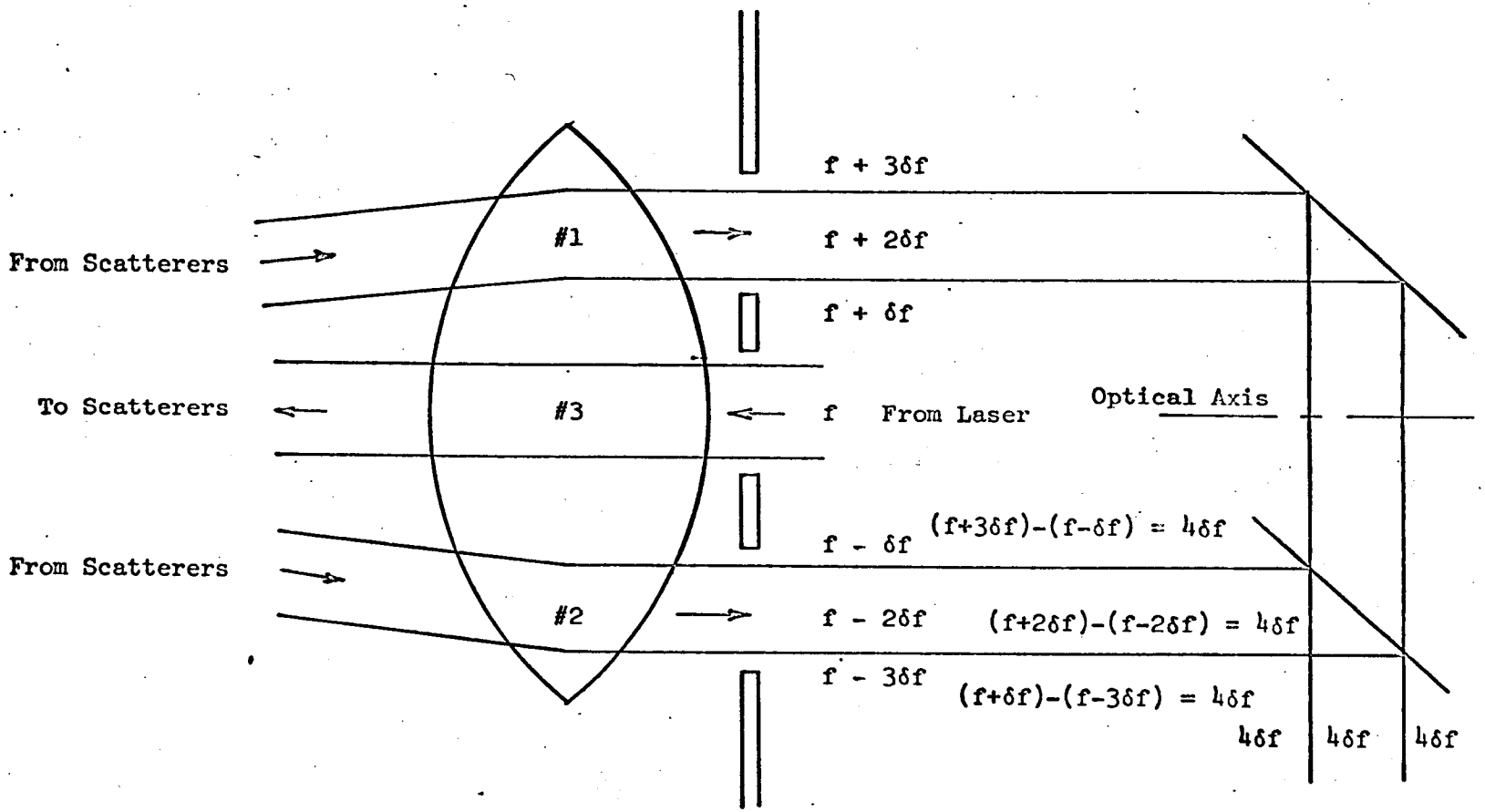

Figure 9

DETAIL OF MIXING ARRANGEMENT FOR OPTICAL HETERODYNE SYSTEM

$$\psi_1 = \psi + \frac{\theta}{2} = \psi_{max}$$

$$\psi_2 = \psi - \frac{\theta}{2} = \psi min$$

$$\theta_1 = \theta + \frac{\theta}{2} = \theta_{max}$$

$$\theta_2 = \theta - \frac{\theta}{2} = \theta_{min}$$

$$\frac{\theta}{2} = 10 \text{ min}$$

$$\theta = 6^\circ$$

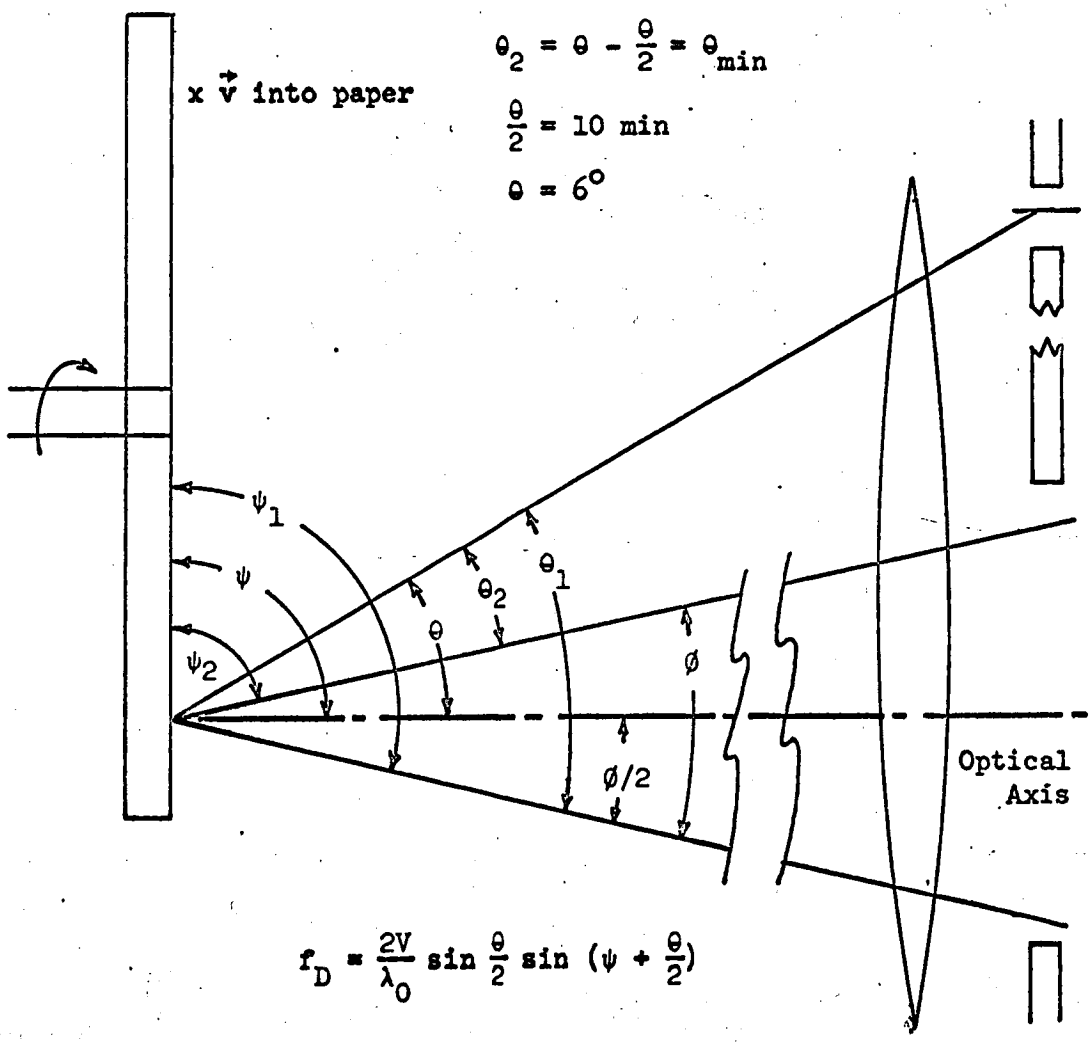

$$f_D = \frac{2V}{\lambda_0} \sin \frac{\theta}{2} \sin \left(\psi + \frac{\theta}{2}\right)$$

Figure 10

DIAGRAM USED IN DERIVATION OF EFFECT
OF BEAM CONVERGENCE ON FREQUENCY SPREAD

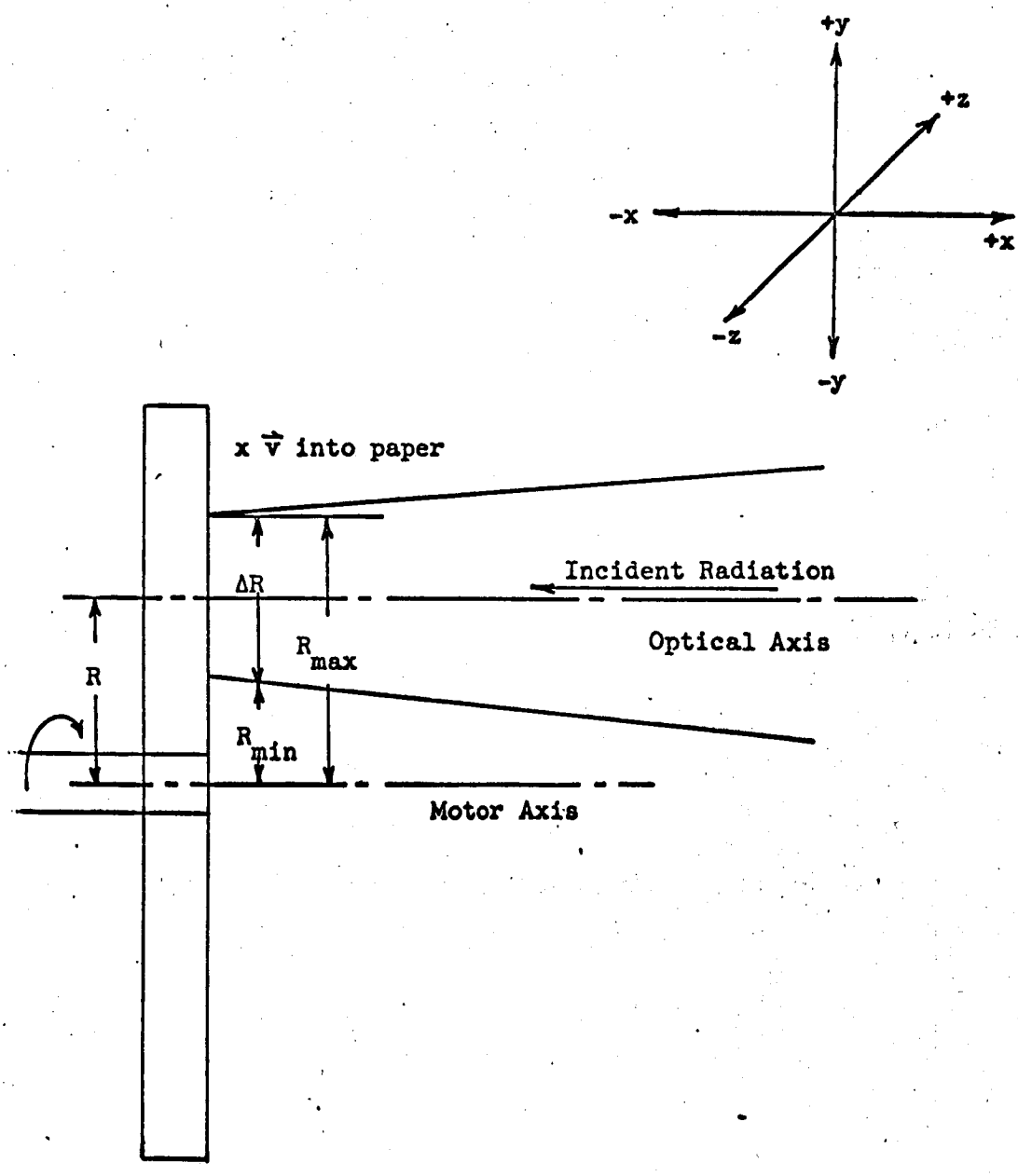

Figure 11

DIAGRAM FOR DERIVATION OF
EFFECT OF VERTICAL DIMENSION OF FOCUSED SPOT ON FREQUENCY SPREAD

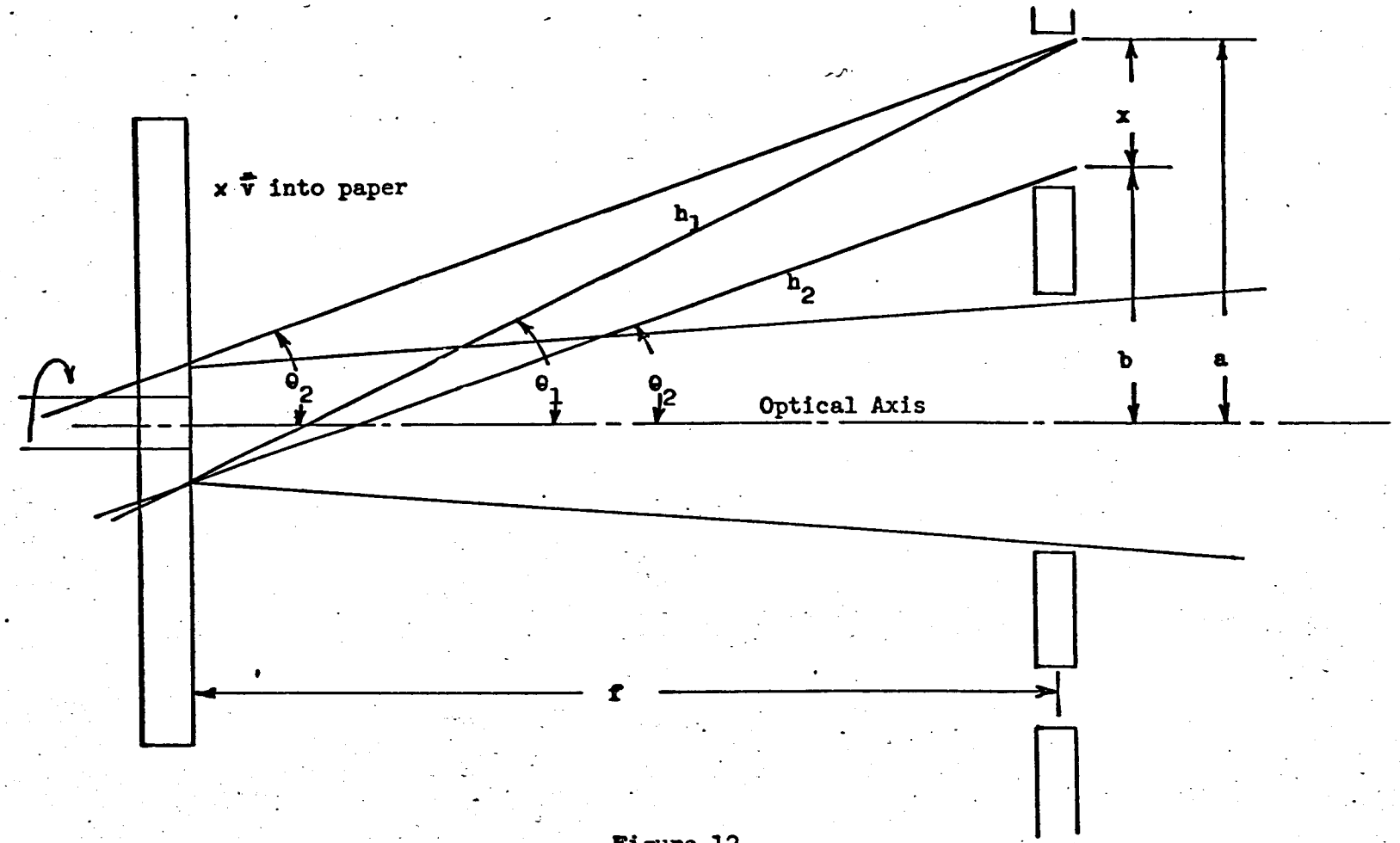

Figure 12

DIAGRAM FOR DERIVATION OF
CONTRIBUTION OF HORIZONTAL BEAM SIZE TO FREQUENCY SPREAD

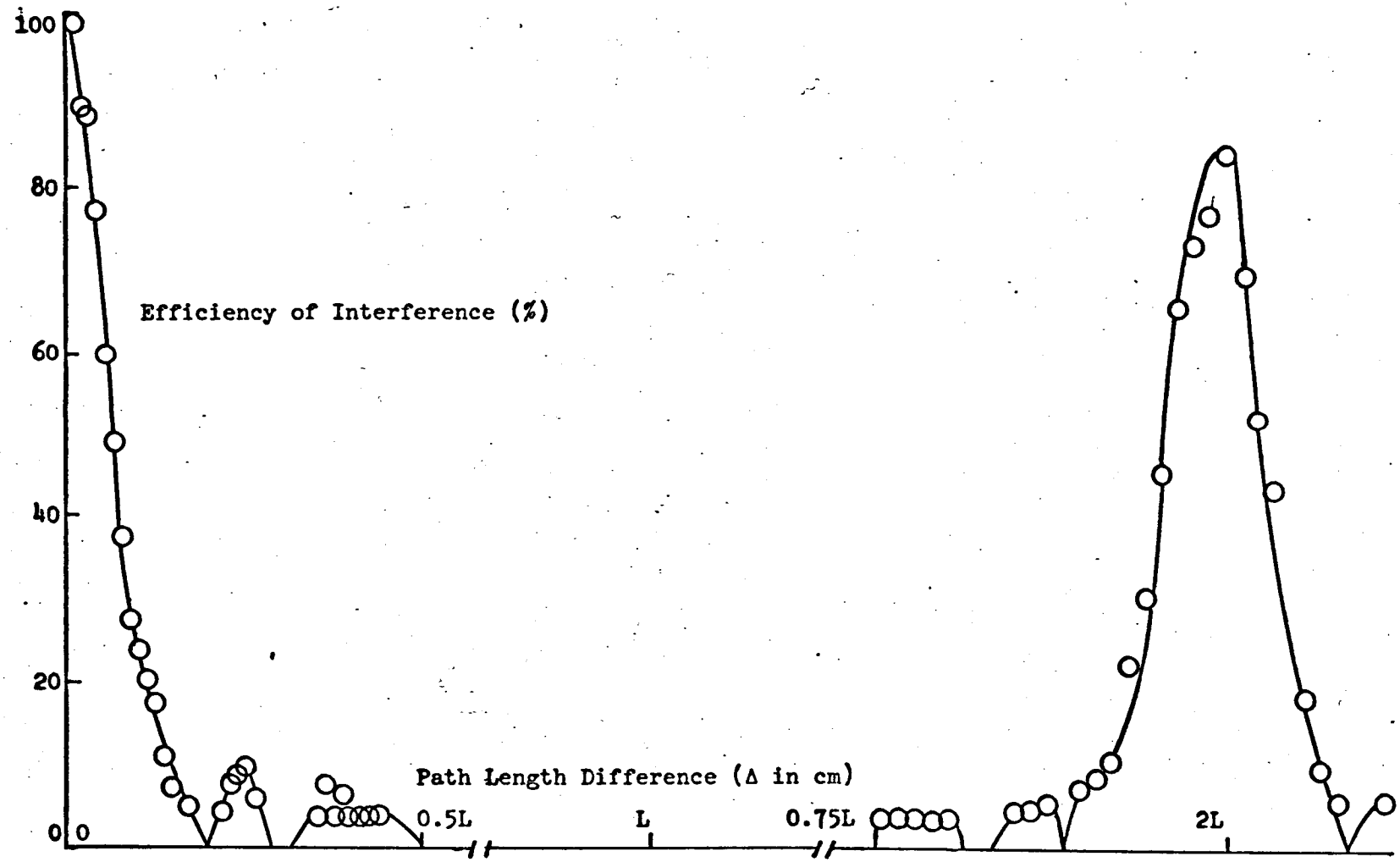

Figure 13

LONGITUDINAL MODE EFFECTS OF SPECTRA PHYSICS MODEL 125. (CAVITY LENGTH L = 180 cm)

A = Dielectric Mirror
B = Lens
C = Dielect Mirror
D = Optical Path Length Compensator To Make Two Legs Optically Equal
E = Cube Beam Splitter

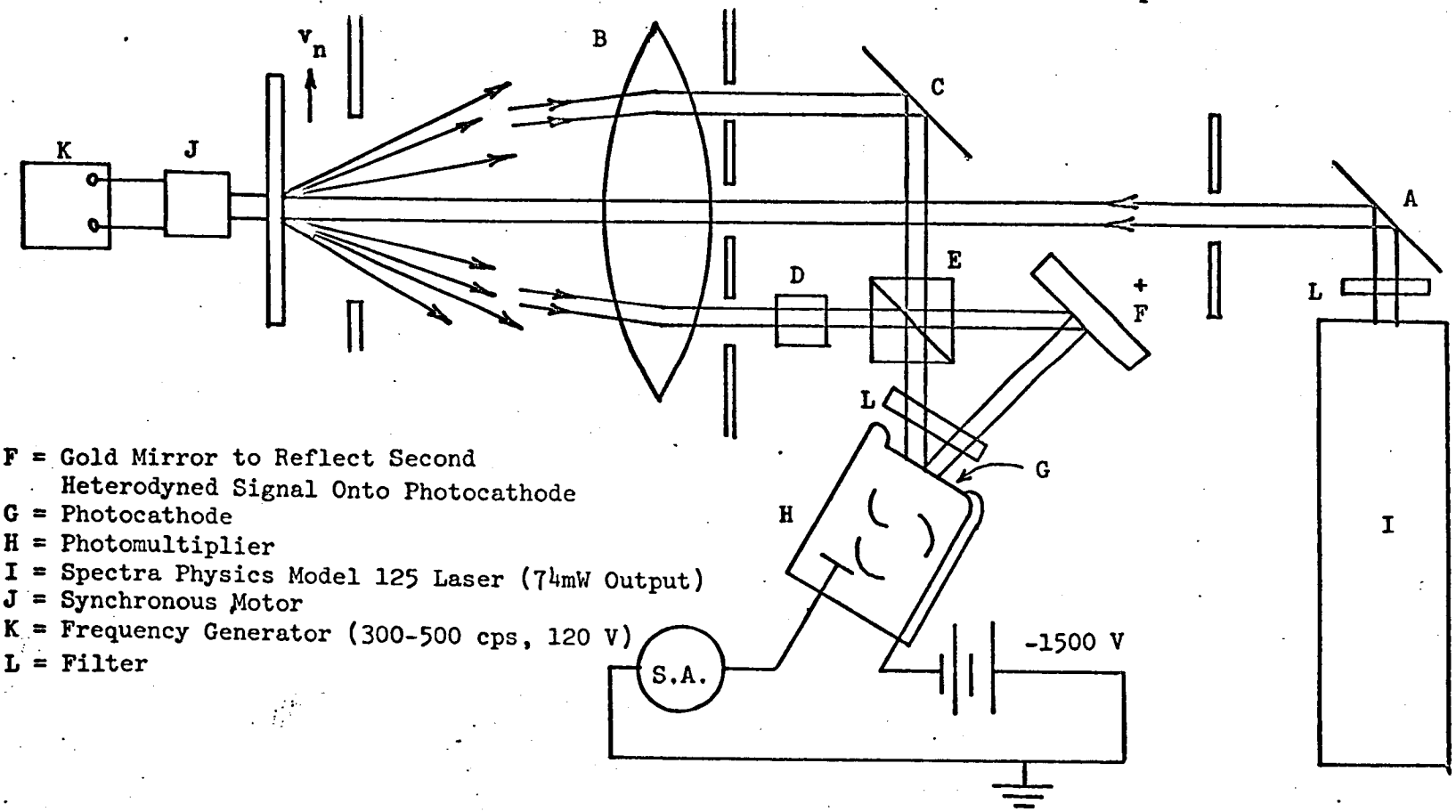

F = Gold Mirror to Reflect Second Heterodyned Signal Onto Photocathode
G = Photocathode
H = Photomultiplier
I = Spectra Physics Model 125 Laser (74mW Output)
J = Synchronous Motor
K = Frequency Generator (300-500 cps, 120 V)
L = Filter

Figure 14

FINAL OPTIMIZED EXPERIMENTAL ARRANGEMENT FOR STUDYING SOLID SCATTERING SYSTEMS